TECHNISCHE UNIVERSITÄT MÜNCHEN

Lehrstuhl für Zoologie

# HCN2 channels in local hippocampal inhibitory interneurons constrain temporoammonic LTP

Lucas M. A. Matt

Vollständiger Abdruck der von der Fakultät Wissenschaftszentrum Weihenstephan für Ernährung, Landnutzung und Umwelt der Technischen Universität München zur Erlangung des akademischen Grades eines

Doktors der Naturwissenschaften

genehmigten Dissertation.

Vorsitzender: Univ.-Prof. Dr. M. Schemann
Prüfer der Dissertation:

1. Univ.-Prof. Dr. H. Luksch
2. apl. Prof. Dr. Th. Kleppisch
3. apl. Prof. Dr. H. Adelsberger

Die Dissertation wurde am 19.04.2010 bei der Technischen Universität München eingereicht und durch die Fakultät Wissenschaftszentrum Weihenstephan für Ernährung, Landnutzung und Umwelt am 07.07.2010 angenommen.

# I Index

# II Figures

# 1 Introduction

## *1.1 The hippocampus and its role in learning and memory*

Perception, cognition and consciousness are commonly considered as fundamental human qualities. However, all three properties could not exist without the ability of the brain to reliably retain information over extended periods of time. For a long time, scholars have been wondering how this remarkable accomplishment is achieved. When neuroscientists successfully started to tackle the problem in the 20th century, one of their most important models for the study of memory was a region of the brain called hippocampus. Up until now, a lot has been learned about the mechanics of information storage in the brain, but there are still many open questions. To date, the hippocampus continues to serve as an outstanding model to study the cellular and molecular events that establish and/or erase memory.

### 1.1.1 Anatomy of the hippocampus

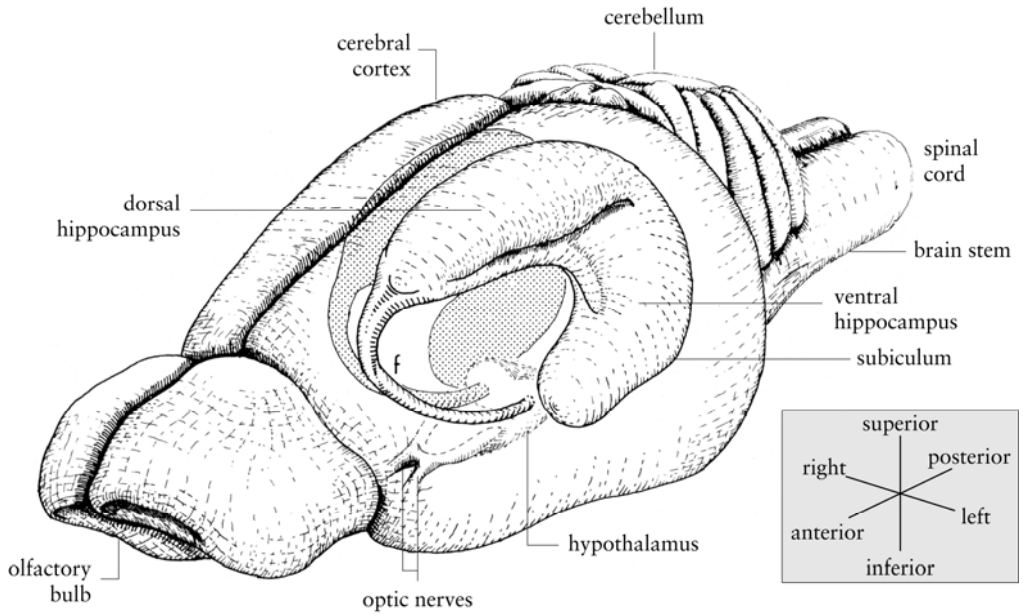


Figure 1: Anatomical location of the hippocampus. This drawing shows the location of the hippocampus in the temporal lobe of the rat brain (modified after Cheung and Cardinal, 2005).

The hippocampal formation is named after the Greek "seahorse" (*hippos* = horse, *kampos* = sea monster). It is located in the medial temporal lobe (Figure 1) and contains cells and neuronal connections that are highly conserved in all mammals. The hippocampal formation can be subdivided into three sections: the *subiculum*, the *dentate gyrus* (**DG**) and the hippocampus proper. The latter is usually referred to as 'the hippocampus' and consists of the four subfields CA1 to CA4 (*cornu ammonis*, the ram's horn, named after its curved shape). Pyramidal cells represent the major population of neuronal cells in the hippocampus proper. Their somas are tightly packed in the *stratum pyramidale* (**sp**) while their dendrites extend through the *stratum radiatum* (**sr**) to the *stratum lacunosum moleculare* (**slm**).

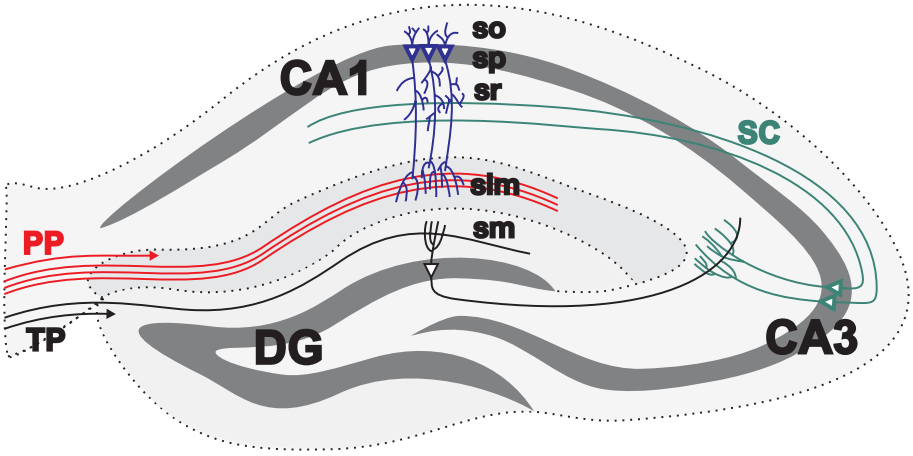


Figure 2: Hippocampal cytoarchitecture. Schematic section transversal to the longitudinal axis of the hippocampus. The major subfields, layers and neuronal connections are indicated. Pyramidal cells of the CA1 are blue, of the CA3 green and granule cells of the **DG** are black. CA1/CA3: *cornu ammonis*; **DG**: *dentate gyrus*; **so**, **sp**, **sr**, **slm**, **sm**: *strata oriens*, *pyramidale*, *radiatum*, *lacunosum moleculare*, and *moleculare*; TP: *tractus perforans*, PP: perforant (temporoammonic) pathway, SC: Schaffer collaterals.

The pyramidal cells of the area CA1 (Figure 2, blue cells) represent the final target of intrahippocampal excitatory connections producing the major glutamatergic output from the hippocampus to the cortex. These cells receive two main excitatory inputs (Figure 2 and Figure 3) from the entorhinal cortex (EC). The first is the trisynaptic pathway. Originating in layer II of the EC (ECII) it relays through the

granule cells of the **DG** and the CA3 pyramidal neurons. The axons of the latter finally terminate at the proximal dendrites of the CA1 pyramidal cells in the **sr** constituting the Schaffer collateral fibers (SC; Figure 2 and Figure 3, green). The second input, the direct perforant or temporoammonic pathway (PP; Figure 2 and Figure 3, red) directly connects from layer III of the entorhinal cortex (ECIII) to the **slm**, where the distal dendrites of the same pyramidal cells are located.

Conveniently all hippocampal connections are oriented in a plane transversal to the longitudinal axis of the hippocampus. This arrangement renders the hippocampus a preferred model for neuroscientists as (*i*) the synaptic connections are reproducibly located and (*ii*) the parallel orientation of the axons in a tissue slice facilitates the simultaneous stimulation and recording of numerous fibers thereby enhancing signal quality in electrophysiological experiments.

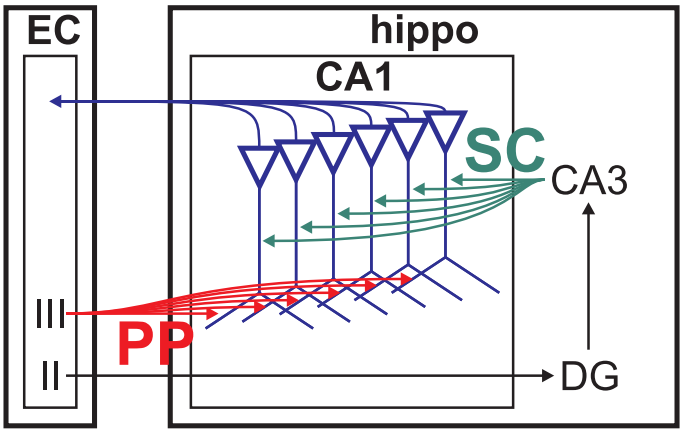


Figure 3: Hippocampal wiring. This simplified model demonstrates the simultaneous innervation of CA1 pyramidal neurons (blue) by the fibers of the Schaffer collateral (SC) and the direct preforant pathway (PP) connecting to proximal and distal dendrites respectively. ECII/ECIII: layer II and III of the entorhinal cortex (EC); **DG**: dentate gyrus; CA1/CA3: *cornu ammonis*; hippo: hippocampus; PP: direct perforant input (red); SC: Schaffer collateral input (green).

Interspersed between the hippocampal layers is a very heterogeneous population of local inhibitory interneurons serving different purposes in local neuronal circuits. Interestingly, interneurons targeting CA1 pyramidal cells can (*i*) mediate feedback or feedforward inhibition, (*ii*) set the threshold for initiation of axonal action

potentials as well as dendritic $Ca^{2+}$ spikes, and (*iii*) participate in the generation of oscillatory activity (Miles et al., 1996; for review see Maccaferri and Lacaille, 2003; Whittington and Traub, 2003; Klausberger, 2009). A major portion of these interneurons is likely represented by oriens-lacunosum moleculare (O-LM) cells (cf. Maccaferri, 2005). Strikingly, they receive glutamatergic input from adjacent CA1 pyramidal cells in close proximity, their axons pass through the **sp** and the **sr** to branch heavily in the **slm**, the site, where the glutamatergic inputs of the PP terminate (Blasco-Ibanez and Freund, 1995; Freund and Buzsaki, 1996; Katona et al., 1999; Maccaferri, 2005; for review see Klausberger, 2009). Consequently, O-LM cells are often regarded as prototypical cells for GABAergic feedback inhibition.

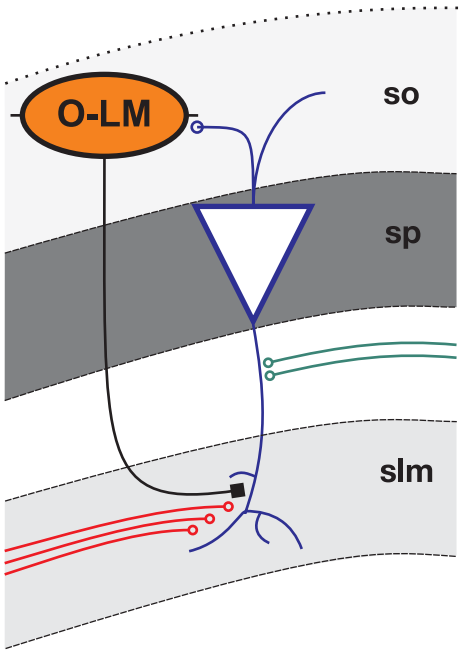


Figure 4: Schematic drawing of an inhibitory feedback circuit involving an oriens-lacunosum moleculare interneuron (O-LM, orange). O-LM cells receive afferents from CA1 pyramidal cells (blue) and relay feedback inhibition to the PP synapses (red) in the *stratum lacunosum moleculare* (**slm**) but not the SC synapses (green) in the *stratum radiatum*. **sp**, **so**: *strata pyramidale* and *oriens*.

### 1.1.2 Function of the hippocampus

For a long time, the mammalian hippocampus has been associated with several aspects of learning and memory (Squire and Zola-Morgan, 1988; Zola-Morgan and Squire, 1993), as patients with damages in the hippocampal formation suffer of severe deficits in their learning ability. Ultimately, the importance of the hippocampus for information storage became clear, when in 1957 William Scoville bilaterally removed the hippocampus of a patient suffering from severe epilepsy resistant to anticonvulsants. After the surgery, the patient later known as 'H.M.' (For a short overview, see Miller, 2009) was relieved from his seizures, but suffered of a striking memory deficit. While H.M. remembered events prior to the surgery to a certain amount, he was unable to form new memories, a condition termed anterograde amnesia. On the other hand, he was able to learn certain motor skills (without any explicit memory of having previously performed the tasks). Obviously the loss of memory was limited to the declarative memory (the memory of facts), while the procedural memory (the acquisition of skills) remained intact. Following these observations, Brenda Milner concluded that the hippocampal formation plays an essential, but time-limited role in the formation of memory without serving as a permanent storage (Milner, 1972).

Another important feature of the hippocampus is its involvement in spatial memory and orientation. Experiments on animals with hippocampal lesions demonstrated for example that the effectiveness of traveling a maze severely depends on the intact function of the hippocampal formation. Work using implanted microelectrodes in freely moving rats documented the existence of place cells that fire according to the animal’s location and advancement in space further demonstra-

ting the importance of the hippocampus in spatial orientation and memory (O'Keefe and Dostrovsky, 1971; O'Keefe and Conway, 1978).

### 1.1.3 Learning and synaptic plasticity

Over a hundred years ago, Santiago Ramón y Cajal (together with Camillo Golgi the winner of the Nobel Prize in Physiology or Medicine, 1905) proposed that dynamic changes in the connections between neurons are the means by which the Brain stores information (Ramón Cajal, 1895). In 1949 this idea inspired Donald O. Hebb, who formulated the principle of plasticity (Hebb, 1949):

> When an axon of cell A is near enough to excite a cell B and repeatedly or persistently takes part in firing it, some growth process or metabolic change takes place in one or both cells such as A's efficiency, as one of the cells firing B, is increased.

Hebb proposes that the transmission efficiency of an individual synapse alters in respect to the quantity and intensity of its activity. Fitting to this hypotheses, Tim Bliss and Terje Lømo evoked long-lasting increases in the efficiency of synaptic transmission using high-frequency stimulation of hippocampal mossy fiber synapses (Bliss and Lomo, 1973). Due to its enduring nature, this increase was termed long-term potentiation (LTP) in contrast to the decrease in transmission strength called long-term depression (LTD) (Douglas and Goddard, 1975). Up to now, different forms of LTP have been demonstrated in a wide variety of glutamatergic synapses (for review see Malenka and Bear, 2004). Additionally, recent work has indeed provided evidence that LTP is a model mechanism of synaptic plasticity correlating with memory formation *in vivo* (Gruart et al., 2006; Whitlock et al., 2006).

One of the best-studied forms of LTP is NMDA (N-methyl-*D*-aspartic acid) receptor dependent LTP in the excitatory synapses to hippocampal CA1 pyramidal neurons. In these synapses, glutamate activates the $Na^+$-permeable AMPA (α-amino-3-

hydroxy-5-methy-4-isoxazolepropionat) receptors leading to excitatory postsynaptic potentials (EPSP) responsible for synaptic transmission. Another iononotropic glutamate receptor present in the postsynaptic membrane is the NMDA receptor that is activated by glutamate only after a blocking $Mg^{2+}$-ion is removed from the channel pore by AMPA-mediated postsynaptic depolarization. Thus, these channels act as hebbian coincidence detectors, sensing the simultaneous activation of the pre- and postsynaptic cell. NMDA receptors initiate LTP by permitting $Ca^{2+}$-entry into the postsynapse (Collingridge et al., 1983; Lynch et al., 1983; Ascher and Nowak, 1986) that subsequently activates the $Ca^{2+}$/calmodulin-dependent kinase II (CamKII) (Giese et al., 1998). CamKII increases the activity and membrane insertion of AMPA receptors via phosphorylation, which ultimately potentiates the respective synapse (Bailey et al., 1996). Furthermore, $Ca^{2+}$ entry triggers protein synthesis allowing the stabilization of the potentiated state of the synapse (Frey et al., 1988).

NMDA receptor activation by removal of the $Mg^{2+}$ block is a crucial step in the initiation of hippocampal LTP, achieved by high frequency stimulation *in vitro*. However, under physiological conditions sufficient depolarization is only elicited through the dendritic integration of excitatory postsynaptic potentials, which is determined by a variety of factors including the function of voltage-gated channels as well as the activity of inhibitory synapses (for review see Magee, 2000; Spruston, 2008).

## *1.2 HCN channels*

### 1.2.1 Structure

The *hyperpolarization-activated cyclic nucleotide-gated cation channels* (HCN) represent a sub-group in the superfamily of voltage-gated pore-loop cation channels (Yu et al., 2005). An HCN channel is assembled of four subunits. Each of the four existing HCN channel subunits carries a transmembrane channel core and an intracellular cyclic-nucleotide binding domain (CNBD). The channel core consists of six membrane-spanning helices (S1-S6). Of these, the positively charged S4 serves as voltage sensor (Vaca et al., 2000), while the extracellular pore-loop between S5 and S6 determines the ion conducting properties of the channel. Upon binding of cyclic adenosine monophosphate (cAMP), the amino-terminal cytoplasmatic CNBD allosterically regulates the function of the channel core (Wainger et al., 2001).

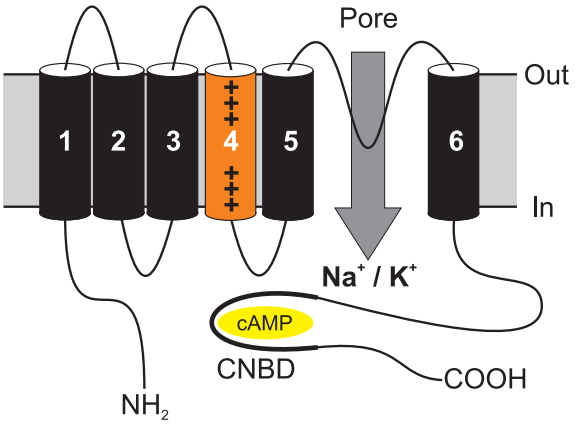


Figure 5: Schematic representation of an HCN channel subunit. 1-6: transmembrane segments S1-S6, CNBD: cyclic nucleotide binding domain, cAMP: cyclic adenosine monophosphate, $NH_2$: amino-terminus, COOH: carboxy-terminus (modified after: Biel et al., 2009).

The highest homology between the four mammalian HCN channel subtypes (HCN1-4) is found in the channel-forming region between S1 and S6. The N- and C-terminal domains show less conservation (Ludwig et al., 1999). In general, the

HCN channel subunits form homotetramers, however some studies also reported the formation of heterotetrameric channels (Ulens and Tytgat, 2001; Much et al., 2003). Additionally, several groups recently reported the tight association of HCN channels with auxiliary subunits responsible for the regulation of intracellular location and activation properties (Lewis et al., 2009; Santoro et al., 2009; Zolles et al., 2009).

HCN1 and HCN2 are the isoforms primarily expressed in CA1 pyramidal neurons with intracellular location restricted to the distal dendrites in the **slm** (Bender et al., 2001; Ludwig et al., 2003; Notomi and Shigemoto, 2004). So far, only few data is available regarding the expression and function of the individual HCN subunits in hippocampal inhibitory interneurons. An immunohistochemical analysis supports the view that HCN1-4 subunits are present in axons and presynaptic terminals of GABAergic interneurons (Notomi and Shigemoto, 2004). Single-cell reverse transcriptase-PCR analysis of fast-spiking basket cells of the dentate gyrus revealed co-expression of HCN1 and HCN2 channels (Aponte et al., 2006). However, the expression of HCN channels in O-LM interneurons remains unclear.

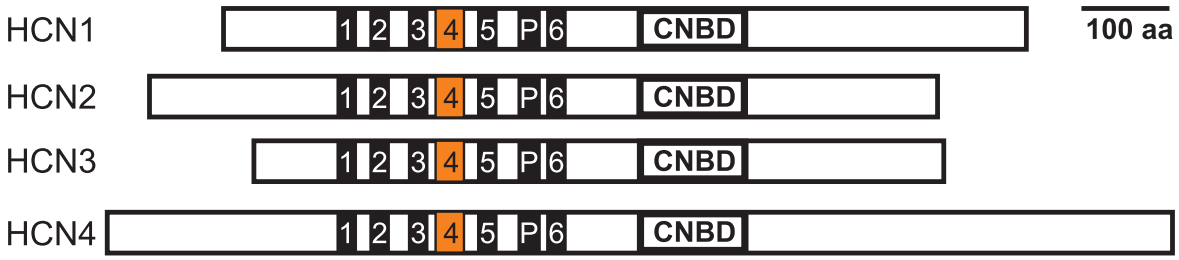


Figure 6: Structural relationship between the HCN channel subtypes. 1-6: transmebrane segments S1-S6; aa: amino acids; CNBD: cyclic nucleotide binding domain; P: pore loop (Modified after Ludwig et al., 1999).

### 1.2.2 Physiology of $I_h$

HCN channels differ from other voltage-gated cation channels in their reversed voltage-dependence that leads to activation upon membrane hyperpolarization

instead of depolarization (Wahl-Schott and Biel, 2009). Inward movement of the charged S4 helix upon hyperpolarized membrane potentials triggers channel opening (Chen et al., 2000), enabling an inwardly directed $Na^+/K^+$ current. This hyperpolarization-activated current was first discovered in cardiac pacemaker cells (Noma and Irisawa, 1976), where it was characterized and termed $I_f$ for "funny current" (Brown et al., 1979). Later, the current was also detected in rod photoreceptors (Bader et al., 1979) and hippocampal pyramidal neurons, where it was termed $I_q$ for "queer" (Halliwell and Adams, 1982). Nowadays the current is generally termed $I_h$ for "hyperpolarization-activated" (Yanagihara and Irisawa, 1980). Molecular cloning of the individual genes established the influence of the four HCN channel subunits on the properties of $I_h$ (Santoro et al., 1997; Gauss et al., 1998; Ludwig et al., 1998). Heterologous expression of the channels revealed that $I_h$ typically activates at membrane potentials more negative than -60 mV. The membrane potential for half-maximal activation ($V_{0.5}$) differs considerably for individual HCN subunits. Characteristic values for $V_{0.5}$ are -70 mV, -95 mV, -77 mV to -95 mV, and -100 mV for HCN1, HCN2, HCN3, and HCN4, respectively (Baruscotti et al., 2005). Interestingly, binding of cAMP induces a +10 mV shift of the voltage-dependency of gating towards more positive potentials in HCN2 and HCN4 channels, while HCN1 and HCN3 are only slightly affected (Viscomi et al., 2001). Milimolar concentrations of $Cs^+$-ions (DiFrancesco, 1982) or several organic blockers (e.g. ivabradine) in low micromolar concentrations almost completely block $I_h$ (Bucchi et al., 2007).

Regarding its unique properties, $I_h$ was assigned the role of a “pacemaker current” responsible for the initiation and regulation of the heart beat (Brown et al., 1977; Yanagihara and Irisawa, 1980). Also in neurons, a number of functions are attributed to $I_h$, such as the generation of rhythmic activity (McCormick and Pape,

1990), the setting of the resting membrane potential (Pape, 1996), dendritic integration (Magee, 2000), and synaptic transmission (Beaumont and Zucker, 2000).

Nolan and coworkers (2004) have provided compelling *in vivo* evidence for the previously suggested role of $I_h$ current-dependent tuning of dendritic integration in behavioral tests (Magee, 1998, 1999). HCN1 channels expressed in a somatodendritic gradient along the dendritic tree of CA1 pyramidal neurons promote a differential impact on the induction of LTP in SC synapses and direct perforant path inputs, respectively. In HCN1 knockout mice ($HCN1^{-/-}$), the loss of HCN1 enhances LTP in the PP but not the SC, paralleled by improved spatial learning of the corresponding mutants (Nolan et al., 2004). The authors concluded that HCN1 channels in the distal dendrites of CA1 pyramidal cells constrain learning by damping postsynaptic changes in membrane potential at these sites, ultimately raising the threshold for triggering synaptic plasticity.

However, the presence of the $GABA_A$ receptor-antagonist picrotoxin in their electrophysiological experiments precluded any possible influence of inhibitory interneurons. Remarkably, $I_h$ currents were detected in distinct types of hippocampal inhibitory interneurons (Maccaferri and McBain, 1996; Ali and Thomson, 1998; Chapman and Lacaille, 1999; Lupica et al., 2001; Aponte et al., 2006). Even more intriguingly, $I_h$ currents can contribute to the inhibition of pyramidal cells by facilitating spontaneous activity and GABA release in *stratum oriens* horizontal interneurons (Lupica et al., 2001).

## *1.3 Conditional mutagenesis of genes using the Cre-loxP system in mice*

To investigate the influence of the HCN2 channel on hippocampal synaptic plasticity and the properties of inhibitory interneurons, genetically modified mouse models were used. Generally, gene deletion in mice is achieved by at least two different gene knockout strategies:

1. The gene of interest is deactivated by a genetic manipulation in the germ line leading to a functional deletion of the gene in every cell (conventional knockout).
2. The gene of interest is manipulated in a tissue specific manner (conditional knockout), usually accomplished by the Cre/loxP system (Cre: cyclization recombination, loxP: locus of X-over P1).

In conventional knockouts, the targeted part of a gene is deleted by homologous recombination with a specific targeting vector in embryonic stem (ES) cells. The manipulated ES cells are injected in blastocysts and subsequently implanted into foster mothers. The resulting chimerical offsprings are backcrossed to wild-type animals enabling germ-line transmission of the targeted gene. Finally, animals homozygous for the mutated allele are generated by mating heterozygous carriers of the targeted gene. The global deletion of functionally important genes can lead to complex phenotypes affecting the whole organism.

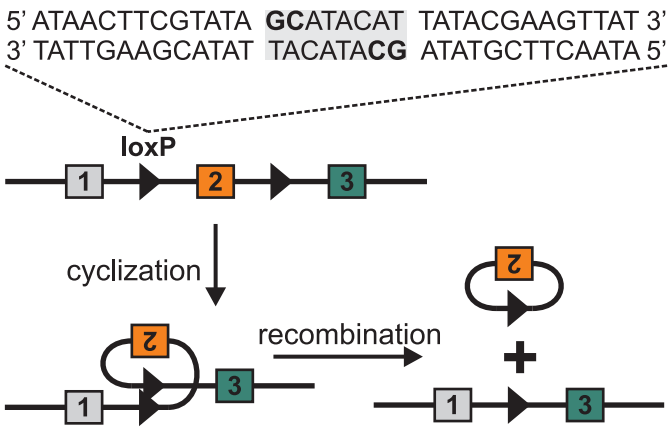


Figure 7: Cre/loxP mediated excision of DNA. The loxP recognition site consists of a core spacer sequence of 8 bp (gray) and two palindromic flanking sequences of 13 bp. Cre cleaves the phosphodiester bonds between the nucleotides in bold type. Recombination between loxP sites in the same orientation results in excision of the flanked DNA segment. Elimination of a circular product is a thermodynamically favorable process.

To overcome these disadvantages, conditional gene deletion by the Cre/loxP system is used (Nagy, 2000). The 38 kDa Cre recombinase is a site-specific DNA recombinase derived from bacteriophage P1. DNA-sequences flanked ("floxed") by two loxP sites (L2) are recognized and excised by this enzyme yielding the L1 knockout allele. Operative in eukaryotic cells, the Cre/loxP system represents a sophisticated tool for tissue or cell-type specific deletion of targeted genes in transgenic mouse models (Lakso et al., 1992; Orban et al., 1992). Analogous to conventional mutagenesis, insertion of loxP sequences into the mouse genome is achieved by homologous recombination in ES cells. Introduction of the loxP sequences into untranscribed exonic sequences ideally retains the expression of wild type protein in animals homozygous for the floxed allele, thereby preventing the emergence of a phenotype. Crossbreeding floxed mice with transgenic animals expressing the Cre recombinase under control of a tissue-specific promoter enables tissue selectivity of the genetic deletion.

## *1.4 Aim of this work*

The goal of the present study was to elucidate the role of the HCN2 channel for synaptic plasticity in glutamatergic inputs to CA1 pyramidal neurons and to evaluate its possible contribution to inhibitory modulation of these inputs. Therefore, the presented data covers (*i*) analysis of the expression pattern of the channel, (*ii*) experimental long-term potentiation (LTP) induced by the Schaffer collateral and direct perforant pathway, (*iii*) recording of spontaneous inhibitory postsynaptic currents (sIPSC) in CA1 pyramidal neurons, and (*iv*) electrophysiological characterizations of O-LM interneurons in preparations from different mouse models lacking the HCN2 and/or the HCN1 channel in all cells or specifically in pyramidal neurons.

# 2 Materials and Methods

Unless indicated otherwise, all chemicals were purchased from Invitrogen (Karlsruhe), Sigma (Schnelldorf), Roth (Karlsruhe), and Millipore (Schwalbach). All primers used in this work were synthesized by Eurofins MWG Operon (Ebersberg).

## *2.1 Experimental Animals*

### 2.1.1 Animal welfare

Animals were maintained and bred in the animal facility of the Institut of Pharmacology und Toxicology, Technische Universität München. Experimental procedures were conducted according to the guidelines of the DFG, the German animal protection laws, and the local government's committee on animal care and welfare in Munich. Mice were maintained at a 12-h light, 12-h dark cycle in type II (5 adult mice) or type III (12 adult mice) Makrolon (Ehret, Emmendingen) cages. Environmental necessities of the laboratory animals were fulfilled by Nestlets as nesting material (Emsicon, Forstinning) and shredded woodchip particles for bedding (Altromin, Lage). Drinking water was provided together with normal chow (Altrumin) ad libidum. Generally, up to two adult females were mated with one male (all of them at least 8 weeks old). DNA for genotyping by PCR (2.1.3) was obtained by tail tip biopsy (0) from 8-14 day old pups. Four-week-old male and female offspring were separated at weaning.

### 2.1.2 Transgenic mouse lines

The genetic background of the mice used in this study was C57BL/6 from Charles River (Sulzfeld) to which all genetically modified strains were backcrossed.

Littermate offspring were used as controls for all experiments performed with mutant mice.

#### 2.1.2.1 HCN1 knockout mouse

Generation and genotyping of mice carrying a genetic deletion of the HCN1 pore-S6 domain has been previously described (Nolan et al., 2003). This mouse line was commercially available from The Jackson Laboratories (Bar Harbor).

#### 2.1.2.2 Floxed HCN2 and HCN2 knockout mouse

Mice carrying loxP-flanked (floxed) exons 2 and 3 of the HCN2 gene (L2) were previously described (Ludwig et al., 2003). Cre recombinase-mediated excision of the floxed sequence (Figure 8) results in a frame shift bringing a stop codon into the reading frame. Mice carrying the global knockout genotype (L1) resulted from crossbreeding L2 mice with a Cre-Deleter mouse that induces germ line recombination of the floxed alleles.

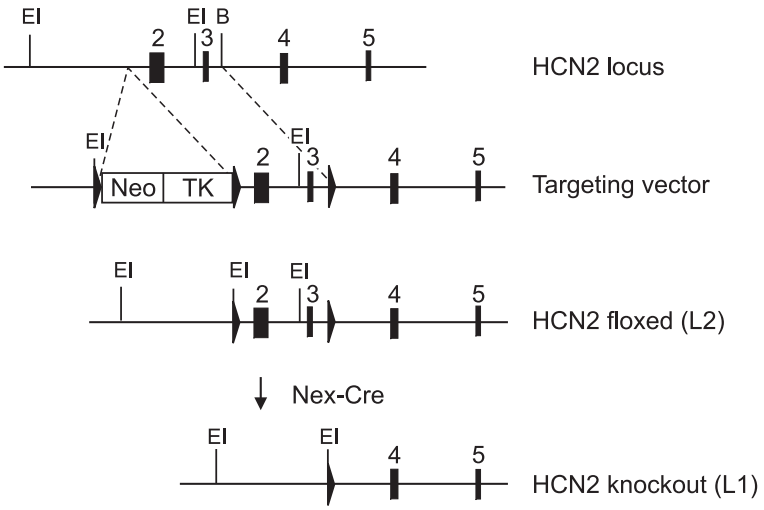


Figure 8: Schematic representation of the mutant HCN2 alleles. The "floxed" L2 allele is converted to the L1 "knockout" allele in cells expressing the Cre recombinase. Numbers depict exons. Triangles stand for loxP sites. EI, B: EcoR1 and BamH1 restriction sites.

#### 2.1.2.3 Pyramidal neuron specific HCN2 knockout mouse

Pyramidal neuron specific conditional knockout mice were generated by cross-breeding mice homozygous for the floxed L2 allele with mice heterozygous for the L1 allele simultaneously carrying the NEX-Cre allele. NEX-Cre mice express Cre recombinase under control of the NEX gene promoter (Schwab et al., 2000). Within the telencephalon NEX expression marks glutamatergic principal neurons and is absent from GABAergic interneurons and macroglial cells (Goebbels et al., 2006). Accordingly, conversion of the conditional HCN2 allele into an HCN2 null allele (L1 allele) is expected to occur in hippocampal CA1 pyramidal cells. The presented breeding plan resulted in the conditional knockout ($HCN2^{PyrKO}$, genotype: $HCN2^{L1/L2}$; $NEX^{+/Cre}$) and the corresponding controls ($HCN2^{PyrCtr}$; genotype: $HCN2^{+/L2}$; $NEX^{+/Cre}$).

#### 2.1.2.4 HCN1 and HCN2 double knockout mouse

Mating of HCN1 and HCN2 knockout mice yielded double mutants (HCN-DKO, genotype $HCN1^{-/-}$; $HCN2^{-/-}$) lacking both the HCN1 and the HCN2 subunit.

### 2.1.3 Genotyping of experimental animals

**Reagents**

1 M Tris-Cl pH 8.0

| | MW [g/mol] | 1 l | c |
|---|---|---|---|
| Tris-Cl | 121.14 | 121.14 g | 1 M |

Add $ddH_2O$ to 1 l. Adjust pH to 8.0 with HCl.

0.5 M EDTA pH 8.0

| | MW [g/mol] | 1 l | c |
|---|---|---|---|
| $Na_2EDTA \cdot 2H_2O$ | 372.24 | 186.1 g | 0.5 M |

Add $ddH_2O$ to 1 l. Adjust pH to 8.0 with HCl.

10x TE buffer

| | 0.5 l | c |
|---|---|---|
| 1 M Tris-Cl pH 8.0 | 50 ml | 0.1 M |
| 0.5 M EDTA pH 8.0 | 10 ml | 10 mM |

Add $ddH_2O$ to 0.5 l.

#### 2.1.3.1 Tail tip biopsy

**Reagents**

Proteinase K (PK) 50 mg/ml in 1x TE buffer
10x Taq DNA Polymerase buffer (Promega)
PK working solution

| | 50 µl | c |
|---|---|---|
| PK (50 mg/ml) in 1xTE buffer | 1 µl | 0.1 M |
| 10x Taq DNA Polymerase buffer | 5 µl | 1x |
| $ddH_2O$ | 45 µl | - |

**Protocol**

For genotyping, 1 mm of mouse tail-tip biopsy material from 8- to 14-day-old animals was used. Tips were incubated over night at 55 °C in 50 µl proteinase K (PK) buffer containing 1 mg/ml PK. Next, samples were centrifuged at 18000 xg for 1 min at room temperature (RT). The supernatant was transferred into a clean polymerase chain reaction (PCR) test tube. Remaining PK activity was inactivated by heating the samples to 95 °C for 15 min. In general, the DNA solution was stored at -20 °C until the genotyping PCR was performed on 1 µl of the samples (2.1.3.2).

### 2.1.3.2 Polymerase chain reaction (PCR)

**Reagents**

1 M KCl

| | MW [g/mol] | 1 l | c |
|---|---|---|---|
| KCl | 74.56 | 74.56 g | 1 M |

Add $ddH_2O$ to 1 l.

1 M $MgCl_2$

| | MW [g/mol] | 0.1 l | c |
|---|---|---|---|
| $MgCl_2 \cdot 6H_2O$ | 203.3 | 20.3 g | 1 M |

Add $ddH_2O$ to 100 ml.

10x PCR buffer

| | stock | 10 ml | c |
|---|---|---|---|
| Tris-Cl pH 8.0 | 1 M | 1 µl | 100 mM |
| $MgCl_2 \cdot 6H_2O$ | 1 M | 0.15 ml | 15 mM |
| KCl | 1 M | 5 ml | 500 mM |
| dNTPs | 100 mM | 0.25 ml each | 2 mM each |

Add $ddH_2O$ to 10 ml.

Promega Taq DNA polymerase (5 U/µl)

**Protocol**

Standard PCR reaction mixture:

| | stock | 25 µl |
|---|---|---|
| Primer A | 25 µM | 0.25 µl |
| Primer B | 25 µM | 0.25 µl |
| Primer C | 25 µM | 0.25 µl |
| PCR buffer | 10x | 2.5 µl |
| Taq DNA polymerase | 5 U/µl | 0.25 µl |
| $ddH_2O$ | - | 20.5 µl |
| DNA (tail biopsy material) | ~100 ng/ml | 1 µl |

As template DNA for genotyping, genomic DNA (approximately 100 ng/ml) isolated from different tail biopsy was used (0). Primer (A, B, C), 10x PCR buffer, Taq DNA

polymerase, and water were calculated for all samples of a reaction and combined to a PCR master mix. 24 µl of the mixture were used together with 1 µl of DNA for the amplification. These standard quantities were varied slightly to improve the quality of the subsequent PCR.

Standard conditions for the amplification:

| | | |
|---|---|---|
| Initial denaturation | 5 min, 94 °C | |
| Denaturation | 15 sec, 94 °C | 35x |
| Annealing | 30 sec, 50-65 °C | |
| Elongation | 30 sec, 72 °C | |
| Final elongation | 5 min, 72 °C | |

These standard conditions vary slightly in dependence on the size of the amplicon and the primer pairs used. Amplification was performed in a Biometra Thermocycler. Sequences of the individual Primers are listed in the Appendix (6.3).

#### 2.1.3.3 Agarose gel electrophoresis

**Reagents**

Ethidium bromide solution (10 mg/ml)
SeaKem LE Agarose (Biozym)
Bromphenol blue

| | 10 l | c |
|---|---|---|
| Bromphenol blue | 0.5 g | 50 mg/ml |

Add $ddH_2O$ to 10 ml.

Xylencyanol FF

| | 10 l | c |
|---|---|---|
| Xylencyanol FF | 0.5 g | 50 mg/ml |

Add $ddH_2O$ to 10 ml.

10x TBE buffer

| | MW [g/mol] | 1 l | c |
|---|---|---|---|
| Tris-Cl | 121.14 | 107.78 g | 0.9 M |
| $Na_2EDTA \cdot 2H_2O$ | 372.24 | 7.44 g | 20 mM |
| Boric Acid | 61.83 | 55 g | 0.9 M |
| Bromphenol blue | 50 mg/ml | 3 ml | 0.15% |
| Xylencyanol FF | 50 mg/ml | 3 ml | 0.15% |

Add $ddH_2O$ to 1 l.

6x DNA loading dye

| | stock | 100 ml | c |
|---|---|---|---|
| Ficoll type 400 | - | 18 g | 18% |
| EDTA, pH 8.0 | 0.5 M | 24 ml | 0.12 M |
| 10x TBE buffer | 10x | 60 ml | 6x |
| Bromphenol blue | 50 mg/ml | 3 ml | 0.15% |
| Xylencyanol FF | 50 mg/ml | 3 ml | 0.15% |

Add $ddH_2O$ to 100 ml.

DNA electrophoresis standard

| | 6ml |
|---|---|
| 1 kb DNA ladder (1 µg/µl) | 100 µl |
| 6x DANN loading dye | 1 ml |
| 10x TE buffer | 0.6 ml |

Add $ddH_2O$ to 6 ml.

**Protocol**

PCR amplified DNA fragments (2.1.3.2) of tail biopsy material (0) DNA were diluted in 6x loading dye. In general, the concentration of agarose in the gel was 2% (w/v) in 1x TBE gel buffer. Gel solutions were heated in a microwave oven before ethidium bromide was added (final concentration was 500 ng/ml). The electrophoresis was done in 1x TBE buffer at 150 V for 30 min depending on the sizes of the fragments to separate.

## *2.2 Western blot analysis*

### 2.2.1 Protein extraction from whole tissue

**Reagents**

1x PBS

SDS lysis buffer

| | stock | 10 ml | c |
|---|---|---|---|
| Tris-Cl pH 8.0 | 1 M | 210 µl | 21 mM |
| SDS | 10% | 670 ml | 0.67% |
| 2-mercaptoethanol | 14.2 M | 170 ml | 238 mM |
| Phenylmethylsulphonyl fluoride | 100 mM | 20 µl | 0.2 mM |

Add dd$H_2O$ to 10 ml.

**Protocol**

To analyze the HCN2 expression in control animals and HCN2$^{PyrKO}$ mice, protein was extracted from different brain regions. Isolated tissue was washed in ice cold 1x PBS and stored at -80 °C until further usage. Frozen tissue was homogenized for 1 min in 1 ml SDS lysis buffer. The homogenates were heated at 95 °C for 10 min and then centrifuged for 5 min at 18000 xg. The supernatant was transferred to a clean test tube. Subsequently proteins were stored at -80 °C until protein concentrations (2.2.2) were determined and Western blot (2.2.3) was performed.

### 2.2.2 Protein quantification assay after Lowry

**Reagents**

Micro Lowry Total protein kit (TP-0300):

Lowry reagent

0.15% (w/v) Deoxycholate solution

72% (w/v) Trichloroacetic acid solution

Folin-Ciocalteu's phenol reagent working solution

Bovine serum albumin (BSA) standard stock solutions (200 µg/ml, 100 µg/ml, 50 µg/ml, 25 µg/ml, 12.5 µg/ml).

**Protocol**

BSA standard was prepared from 200 µl of each BSA standard stock solution, which were diluted with dd$H_2O$ to a final volume of 1 ml. Protein samples were heated at 95 °C for 5 min. dd$H_2O$ was added to a final volume of 1 ml to 2-30 µl denaturated extract. As reference, an equal volume of lysis buffer was used in water. Blank samples (water only) were included in every assay. For precipitation, 100 µl deoxycholate (1.5 mg/ml) were added to each reaction. After mixing, solutions were incubated for 10 min at RT. Next, 100 µl trichloroacetic acid solution (72%) were added and all tubes were mixed immediately. Precipitated proteins were isolated through a centrifugation step of 10 min at 18000 xg after which the supernatant was discarded and the pellet dissolved in 200 µl Lowry reagent. After adding 200 µl of dd$H_2O$, solutions were mixed well and incubated for 20 min at RT. Eventually, 100 µl Folin-Ciocalteu's phenol were added. Color developed within 30 min incubation at RT. Solutions were transferred to cuvettes and the absorbance was determined at a wavelength of 750 nm. Protein concentrations were calculated from the standard curve.

### 2.2.3 Immunoblotting

**Reagents**

4x Tris-Cl-SDS, pH 6.8/pH 8.8

| | MW [g/mol] | 100 ml | c |
|---|---|---|---|
| Tris-Cl | 121.14 | 6.05 g | 0.5 M |
| SDS | 288.38 | 0.4 g | 0.4% |

Add dd$H_2O$ to 100 ml. Adjust pH 6.8 or pH 8.8 with HCl.

6x SDS sample buffer

| | 10 ml |
|---|---|
| 4x Tris-Cl-SDS, pH 6.8 | 7 ml |
| Glycerol | 3.6 g |
| SDS | 1 g |
| 1,4-Dithiothreitol (DTT) | 0.93 g |
| Bromphenol Blue | 1.2 mg |

Add $ddH_2O$ to 10 ml.

Separating gel/Stacking gel

| | separating gel 8% | stacking gel |
|---|---|---|
| 30% acrylamide, 0.8% bisacrylamide solution | 4 ml | 4.5 ml |
| 4x Tris-CL-SDS, pH 8.8 | 3.75 ml | 3.75 ml |
| $ddH_2O$ | 7.25 ml | 6.75 ml |
| 30% ammonium persulfate (APS) | 50 µl | 50 µl |
| N,N,N',N'-tetramethylethylenediamine (TEMED) | 10 µl | 10 µl |

10x SDS electrophoresis buffer

| | MW [g/mol] | 1 l | c |
|---|---|---|---|
| Tris-Cl | 121.14 | 30.03 g | 250 mM |
| Glycine | 75.07 | 144.1 g | 1.92 M |
| SDS | 288.38 | 10.0 g | 1% |

Add $ddH_2O$ to 1 l.

Anode transfer buffer-I, pH 10.4

| | MW [g/mol] | 1 l | c |
|---|---|---|---|
| Tris-Cl | 121.14 | 36.3 g | 0.3 M |
| Methanol (MeOH) | 100% | 200 ml | 20% |

Dissolve Tris-Cl in 800 ml $ddH_2O$, adjust to pH 10.4. Add 200 ml MeOH.

Anode transfer buffer-II, pH 10.4

| | MW [g/mol] | 1 l | c |
|---|---|---|---|
| Tris-Cl | 121.14 | 3.03 g | 20 mM |
| Methanol (MeOH) | 100% | 200 ml | 20% |

Dissolve Tris-Cl in 800 ml $ddH_2O$, adjust to pH 10.4. Add 200 ml MeOH.

Cathode transfer buffer, pH 7.6

| | MW [g/mol] | 1 l | c |
|---|---|---|---|
| Tris-Cl | 121.14 | 3.03 g | 20 mM |
| 6-Aminocaproic acid | 131.18 | 5.2 g | 40 mM |
| Methanol (MeOH) | 100% | 200 ml | 20% |

Dissolve Tris-Cl in 800 ml $ddH_2O$, adjust to pH 7.6. Add 200 ml MeOH.

10x TBS, pH 8.2

| | MW [g/mol] | 1 l | C |
|---|---|---|---|
| Tris-Cl | 121.14 | 6.05 g | 50 mM |
| NaCl | 58.44 | 43.8 g | 750 mM |
| Methanol (MeOH) | 100% | 200 ml | 20% |

Dissolve Tris-Cl in 800 ml $ddH_2O$, adjust to pH 8.2. Add 200 ml MeOH.

1x TBS-T (0.1% Tween)

| | 500 ml |
|---|---|
| 10x TBS | 50 ml |
| Tween20 | 0.5 ml |

Add $ddH_2O$ to 500 ml.

1x TBS-T blocking solution (5% milk powder)

1x TBS-T washing solution (1% milk powder)

Molecular weight standards:

- See-Blue (Invitrogen)
- See-Blue Plus2 (Invitrogen)

Polyvinyliden difluoride (PVDF) membrane (Millipore)

ECL Western blotting analysis system (Amersham):

- Detection reagent A
- Detection reagent B

**Protocol**

After quantification, the final concentration of the extracts was adjusted to 1-2 µg/µl protein in 2x SDS sample buffer by diluting the extracts with 6x SDS

sample buffer in dd$H_2O$. Generally, samples of 10-30 µg protein were loaded on a gel after boiling at 95 °C for 5 min. Proteins were separated by their molecular weight using denaturing SDS polyacrylamide gel (8-9%) electrophoresis. Next, the separated proteins were transferred (blotted) to a polyvinyliden difluoride (PVDF) membrane using a semi-dry transfer chamber.

The setup of the blotting chamber was:

(1.) anode plate, (2.) 3x filter papers saturated with anode transfer buffer-I, (4.) 2x filter papers saturated with anode transfer buffer-II, (5.) PVDF membrane soaked in 100% methanol and saturated with anode transfer buffer-II, (6.) gel, (7.) 5x filter papers saturated with cathode transfer buffer, and (8.) cathode plate. The transfer was performed for 1 h at 50 mA for each gel.

Unspecific binding of the antibodies to the membrane was blocked with 5% milk powder in 1x TBS-T for 1 h at RT. The membrane was then exposed sequentially to solutions containing the primary antibodies (over night at 4 °C), followed by the horseradish peroxidase (HRP) conjugated secondary antibodies (RT for 45 min) diluted 1:2000 in 1.0% milk powder in 1x TBS-T. In between incubations with blocking-, primary-, and secondary-antibody solutions the membrane was regularly washed with three changes of 1% milk powder in 1x TBS-T. Before soaking the membrane in the detection reagent to enable a color reaction, another washing was done with three changes of 1x TBS-T only. The enhanced chemiluminescent (ECL) method was used for detection of the antigen-antibody complexes. 1 ml of a 1:1 mixture of the detection solutions A and B was used for each membrane. Following exposure of the soaked membrane to an X-ray film, the protein antigen was visualized as a band. A molecular weight standard containing proteins of known size provided information about the molecular weight of the protein.

## *2.3 Immunohistochemistry*

### 2.3.1 Cryo sectioning of mouse brains

**Reagents**

2-Methyl-pentane
Dry ice
Ethanol
Diethyl-ether

**Protocol**

A beaker filled with 2-methyl-pentane was submerged in dry-ice cooled ethanol. 12-week-old mice were decapitated after diethyl-ether anesthesia; their brains were removed and immediately shock-frozen in about -40 °C cold 2-methyl-butane. Deep-frozen brains were stored at -80 °C until they were cut in a cryostat to 12 µm thick coronal sections. Tissue slices were thaw-mounted on Polysine glass-slides (Menzel, Braunschweig), air-dried and stored at -20 °C until used.

### 2.3.2 Immunohistochemical staining

**Reagents**

1x PBS
Paraformaldehyde solution

| | 0.1 l | c |
|---|---|---|
| PFA | 4 g | 1 M |

Dissolve in 100 ml 1x PBS, pH 7.4 at 60 °C.

Permeabilization and blocking solution

| | 2 ml | c |
|---|---|---|
| BSA | 40 mg | 2% |
| Triton X-100 (3%) | 200 µl | 0.3% |
| Normal goat serum (NGS) | 100 µl | 5% |

Add 1x PBS, pH 7.4 to 2 ml.

Peroxidase quenching solution

| | 50 ml | c |
|---|---|---|
| $H_2O_2$ (30%) | 5 ml | 3% |

Add dd$H_2O$ to 50 ml

Hoechst 33342 (Fluka)
PermaFluor aqueous mounting medium (Beckman Coulter)

**Protocol**

All reagents were applied to the individual sections using a micropipette. Unless otherwise indicated, all steps were performed at room temperature. All procedures that included fluorescent dyes were performed in the dark. The glass slides carrying the slices were thawed and incubated in PBS for rehydration. After isolating single sections with a PAP-pen (DAKO), the slides were placed in a custom-made wet-chamber. First, the sections were fixed for 5 min in paraformaldehyde solution. After washing in PBS the permeabilization and blocking buffer was applied for 90 min. After a washing step, the slices were incubated with the primary antibodies overnight at 4 °C in PBS (1% BSA). After washing, endogenous peroxidase activity was quenched for 10 min to reduce the background signal for the Tyramide Signal Amplification (TSA). Subsequently the slides were thoroughly washed. Secondary antibodies were applied in PBS (2% normal goat serum) for 60 min. In order to intensify the fluorescent signal of the HCN channels, a TSA kit (Perkin Elmer, Waltham) was used. This method takes

advantage of a fluorescent substrate immobilized by the activity of peroxidase enzyme coupled to the secondary antibody. For TSA, slices were washed in PBS first, and then the buffer was changed to 1x TBS for a minute before a 1 min preincubation with TSA-buffer (from Perkin-Elmer kit). Care was taken to restrict the incubation time of the tyramide solution (1:200 in TSA-buffer) to equal durations (8 min) for every slice. After an additional washing step the sections were incubated for 5 min in Hoechst 33342 (5 µg/ml) to counterstain cell nuclei. Sections were mounted with PermaFluor and cover-slides.

**Imaging**

Immunohistochemically stained brain slices were imaged using an LSM 510 Meta confocal laser scanning microscope (Zeiss, Germany). Raw data from the microscope was analyzed using the Zeiss LSM Image Browser software. To avoid misinterpretation, the same adjustments for brightness and contrast were applied to all images from a dataset.

## *2.4 Electrophysiology*

### Reagents

Carbogen – 95% $O_2$, 5% $CO_2$

Artificial cerebrospinal fluid (aCSF)

| | MW [g/mol] | 5 l | c |
|---|---|---|---|
| D-Glukose | 198.17 | 9.909 g | 10 mM |
| KCl | 74.56 | 1.118 g | 3 mM |
| NaCl | 58.44 | 36.233 g | 124 mM |
| $NaHCO_3$ | 84.01 | 10.921 g | 26 mM |
| $KH_2PO_4$ | 136.09 | 0.851 g | 1.25 mM |
| $CaCl_2$ | 147.02 | 1.838 g | 2.5 mM |
| $MgSO_4 \cdot 7H_2O$ | 246.48 | 2.465 g | 2 mM |

Add dd$H_2O$ to 5 l. Constantly bubble with carbogen. Adjust to pH 7.4 with HCl / NaOH.

### 2.4.1 Preparation of acute slices

Mice (8- to 12-week-old for fEPSP, 2-week-old for whole-cell patch-clamp experiments) were deeply anesthetized with diethyl-ether and then decapitated. Subsequently the brains were removed.

For fEPSP recordings, the hippocampi were dissected. Using an egg-slicer (Katz, 1987), transverse slices (400 µm thick) were prepared and then kept at room temperature for ≥1.5 hours in aCSF that was constantly bubbled with carbogen (95% $O_2$, 5% $CO_2$).

To obtain slices for whole-cell patch-clamp recordings the cerebellum was removed from the dissected brain. The edge of the cut was glued to the specimen holder using household cyanoacrylate adhesive. Using a vibration microtome (Microm) equipped with a single-use steel razorblade the brain was sliced in 200-300 µm thick coronal sections. After transfer to aCSF bubbled with carbogen the slices were kept at room temperature for up to 8 hours.

### 2.4.2 Field EPSP (fEPSP) recordings in hippocampal slices

**Reagents**

Carbogen
aCSF
Picrotoxin (PiTX)

**Protocol**

To record fEPSPs in the SC pathway, stimulating and recording electrodes were positioned within the *stratum radiatum* near the CA3 region and in the CA1 region, respectively. To obtain selective postsynaptic responses of perforant path inputs, stimulating and recording electrodes were placed in the distal region of the *stratum lacunosum moleculare* (Figure 9).

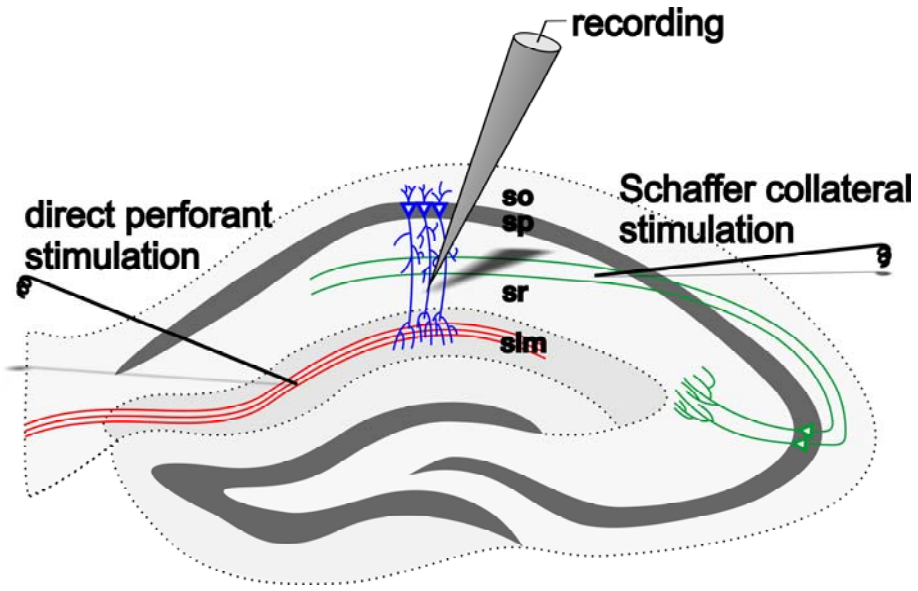


Figure 9: Figure depicting the position of recording and stimulating electrodes during fEPSP experiments. The drawing approximates the position of the recording electrode in the *stratum radiatum* (**sr**) and the stimulating electrode in the **sr** proximal to the CA3 region or the *stratum lacunosum moleculare* (**slm**) for SC or TA stimulation respectively. **so**, **sp**: *strata oriens* and *pyramidale*.

As recording electrodes for fEPSPs, aCSF-filled glass pipettes (~3 MΩ) prepared with a P-97 horizontal puller (Sutter Instruments, Novato) were used. Stimulation and data acquisition through an Axoclamp 2B amplifier (Axon Instruments, USA)

were controlled by PULSE software (HEKA, Lambrecht/Pfalz) via an ITC-16 computer interface (Instrutech, Longmont). Stimuli (100 µs) were delivered through a concentric bipolar electrode connected to an A360 stimulus isolator (World Precision Instruments, Sarasota). The same intensity was used during baseline recording and induction of LTP using 4 trains of 50 stimuli @ 100 Hz separated by 10 s. When indicated, 50 µM picrotoxin was washed into the bath solution.

### 2.4.3 Whole-cell patch-clamp recording

#### 2.4.3.1 $I_h$ isolation and current-clamp

**Reagents**

aCSF
Caesium chloride
Zatebradine (Tocris)
Intracellular solution

| | MW [g/mol] | 100 ml | c |
|---|---|---|---|
| D-Glukose | 198.17 | 0.198 g | 10 mM |
| HEPES | 238.31 | 0.238 g | 10 mM |
| K-Gluconate | 234.20 | 2.225 g | 95 mM |
| $K_3$-Citrate | 306.4 | 0.613 g | 20 mM |
| NaCl | 58.44 | 0.058 g | 10 mM |
| $CaCl_2$ | 147.02 | 0.007 g | 0.5 mM |
| $MgCl_2 \cdot 6H_2O$ | 203.3 | 0.020 g | 1 mM |
| EGTA | 380.4 | 0.001 g | 0.02 mM |
| KATP | 583.4 | 0.058 g | 1 mM |
| $Na_2GTP$ | 523.2 | 0.026 g | 0.5 mM |

Add dd$H_2O$ to 100 ml. Adjust to pH 7.4 with HCl / NaOH.

**Protocol**

For recording, acute brain slices (2.4.1) were placed in a recording chamber continuously perfused with aCSF bubbled with carbogen at room temperature.

Hippocampal interneurons and pyramidal cells were visually identified under an upright microscope (Olympus, Hamburg) with DIC contrast (Dodt and Zieglgansberger, 1990). Patch pipettes (2-3.5 MΩ) were pulled from borosilicate glass capillaries using a horizontal P-97 puller (Sutter). All patch-clamp recordings were made in the whole-cell configuration using an EPC-9 amplifier and the PULSE software (HEKA). In O-LM cells current-clamp recordings of the membrane potential and voltage-clamp recordings of $I_h$ currents were performed. The extracellular solution in these experiments consisted of aCSF, supplemented with zatebradine or CsCl (4 mM) where indicated. $I_h$ currents were recorded in cells held at -45 mV during 2 s voltage-clamp steps to hyperpolarizing test potentials of -55 mV to -125 mV followed by a final step to -125 mV, a potential causing nearly complete activation.

Current fractions activating during hyperpolarization were fitted to the following function: $I_{act}(V) = G_{rel} * (V-V_{rev}) / (1+\exp((V-V_{1/2})/k)$, where $G_{rel}$ is a relative conductance, V the test potential, $V_{rev}$ the reversal potential calculated using to the Goldmann-Hodgkin-Katz equation, $V_{1/2}$ the potential corresponding to the midpoint of activation and k a slope factor. More accurate determination of the voltage-dependence of $I_h$ current activation was obtained based on the amplitude of instant tail currents ($I_{tail}[V]$) elicited during the voltage-clamp step to -125 mV following individual test pulses. The instant tail current is maximal ($I_{max}$) following the test pulse to -125 mV (full activation during test pulse), and minimal ($I_{min}$) following the test pulse to -45 mV (no activation during preceding test pulse). The voltage-dependence of $I_h$ current activation can be described by the following Boltzmann function: $(I_{tail}[V] – I_{min}) / (I_{max} – I_{min}). = 1 / (1 + \exp[(V-V_{1/2})/k] )$.

The input resistance of O-LM cells is represented by the slope derived from a linear regression analysis between the steady state membrane potential ($V_{SS}$) and

the corresponding current injections during small current-clamp steps in hyper- and depolarizing direction.

#### 2.4.3.2 sIPSC recordings

**Reagents**

aCSF
6,7-Dinitroquinoxaline-2,3-dione (DNQX)
(*2R*)-amino-5-phosphonopentanoate (AP-5)
Zatebradine
*S*-(3,5)-dihydroxyphenylglycine (DHPG)
PiTX
Intracellular solution for sIPSC

| | MW [g/mol] | 100 ml | c |
|---|---|---|---|
| CsCl | 168.4 | 2.105 g | 125 mM |
| HEPES | 238.31 | 0.238 g | 10 mM |
| EGTA | 380.4 | 0.038 g | 1 mM |
| $CaCl_2$ | 147.02 | 0.001 g | 0.1 mM |
| $MgCl_2$ | 95.2 | 0.038 g | 4 mM |
| $Na_2ATP$ | 507.2 | 0.101 g | 2 mM |
| $Na_2GTP$ | 523.2 | 0.010 g | 0.2 mM |

Add dd$H_2O$ to 100 ml. Adjust to pH 7.4 with HCl / CsOH.

**Protocol**

Whole-cell voltage-clamp recordings using the EPC-9 amplifier were made from the soma of visually identified CA1 pyramidal neurons to measure spontaneous inhibitory postsynaptic currents (sIPSC). sIPSC were isolated pharmacologically from other synaptic currents by supplementing the standard extracellular solution (aCSF) with 25 µM DNQX and 50 µM AP-5. The $Cl^-$ reversal potential was about 0 mV, and CA1 pyramidal neurons were held at -70 mV. Under these conditions, the spontaneous activation of postsynaptic GABA receptors leads to a transient inward current. The HCN channel blocker zatebradine or DHPG, an agonist of

Group I metabotropic glutamate receptors were supplemented for experiments. Routinely, picrotoxin (50 µM) was added at the end of these experiments to confirm that the observed synaptic currents were GABAergic.

#### 2.4.3.3 Recording of spontaneous activity

**Reagents**

aCSF
Kynurenic acid (KYNA)
Zatebradine
Intracellular solution

| | MW [g/mol] | 100 ml | c |
|---|---|---|---|
| D-Glukose | 198.17 | 0.198 g | 10 mM |
| HEPES | 238.31 | 0.238 g | 10 mM |
| K-Gluconate | 234.20 | 2.225 g | 95 mM |
| $K_3$-Citrate | 306.4 | 0.613 g | 20 mM |
| NaCl | 58.44 | 0.058 g | 10 mM |
| $CaCl_2$ | 147.02 | 0.007 g | 0.5 mM |
| $MgCl_2 \cdot 6H_2O$ | 203.3 | 0.020 g | 1 mM |
| EGTA | 380.4 | 0.001 g | 0.02 mM |
| KATP | 583.4 | 0.058 g | 1 mM |
| $Na_2GTP$ | 523.2 | 0.026 g | 0.5 mM |

Add $ddH_2O$ to 100 ml. Adjust to pH 7.4 with HCl / NaOH.

**Protocol**

Whole-cell voltage-clamp recordings using the EPC-9 amplifier were made from the soma of visually identified **so** interneurons in acute slices. Kynurenic acid (2 mM) was routinely added to the bath solution as broadband antagonist of glutamatergic transmission. This allowed measurement of spontaneous intrinsic action potential activity free from excitatory synaptic events. Under conditions of no current injection, ~$^1/_3$ of O-LM cells exhibited spontaneous spiking activity

which was examined in the absence and in the presence of zatebradine (Maccaferri and McBain, 1996).

#### 2.4.3.4 Post-hoc staining of biocytin-filled interneurons

**Reagents**

Biocytin

Vectastain peroxidase (ABC-Peroxidase) elite standard kit (Vector Laboratories)

| | 10 ml |
|---|---|
| Reagent A (Avidin DH) | 100 µl |
| Reagent B (Biotinylated peroxidise) | 100 µl |

Add 1x PBS, pH 7.4 to 10 ml. Incubate 30 min before use in the dark.

PBS

Paraformaldehyde solution

| | 0.1 l | c |
|---|---|---|
| PFA | 4 g | 1 M |

Dissolve in 100 ml 1x PBS, pH 7.4 at 60 °C.

3,3'-diaminobenzidine tetrahydrochloride (DAB) stock solution

| | 50 ml | c |
|---|---|---|
| PFA | 50 mg | 0.1 % |

Add 1x PBS, pH 7.4 to 50 ml.

DAB staining solution

| | stock | 10 ml | c |
|---|---|---|---|
| DAB | 0.1% | 5 ml | 0.05% |
| $H_2O_2$ | 30% | 10 µl | 0.03% |

Add 1x PBS, pH 7.4 to 10 ml.

Permeabilization solution

| | 50 ml | c |
|---|---|---|
| Triton X-100 (3%) | 1.5 ml | 3% |

Add 1x PBS, pH 7.4 to 50 ml.

Peroxidase quenching solution

| | 50 ml | c |
|---|---|---|
| $H_2O_2$ (30%) | 5 ml | 3% |

Add dd$H_2O$ to 50 ml

Aquatex mounting medium (VWR)

**Protocol**

1-2 mg/ml biocytin was dissolved in the intracellular solution and diffused into the cell during patch-clamp experiments. For subsequent steps the slices were placed in a 32-well plate. Fixation in paraformaldehyde solution took place overnight at room temperature. Biocytin was visualized using the ABC-Peroxidase kit with DAB as substrate. To achieve this, brain slices were washed 3x5 min in PBS. Membranes were permeabilised by 30 min incubation and washed 3x 2 min in PBS. Endogenous peroxidase was quenched for 10 min, followed by an additional washing step (3x 2 min in PBS). After this, biocytin was targeted for 75 min with the streptavidin-peroxidase- (ABC-) complex in the dark. Following a 3x 2 min washing in PBS, the slices were incubated in DAB staining solution until brown deposit became visible. Finally, slices were washed in PBS, mounted on glass-slides using Aquatex and visualized by a bright-field microscope.

### 2.4.4 Data analysis

All data are represented as mean ± SEM. All LTP experiments show the slope of an averaged postsynaptic response. Routinely, four consecutive fEPSPs (corresponding to 1 min) were averaged. For statistical analysis of LTP, the average values during the last five minutes of the hour following tetanus were compared using Student's t-test. Analysis of patch-clamp data was performed using PULSE/PULSEFIT (HEKA, Germany) and Origin 6.1 (OriginLab, USA) including custom routines. Spontaneous spiking activity and spontaneous IPSCs

were analyzed using MiniAnalysis package (Synaptosoft, USA). Significance levels are indicated by asterisks (* $p < 0.05$, ** $p < 0.01$, *** $p < 0.001$).

# 3 Results

## 3.1 Expression of HCN1 and HCN2 channels in the hippocampus

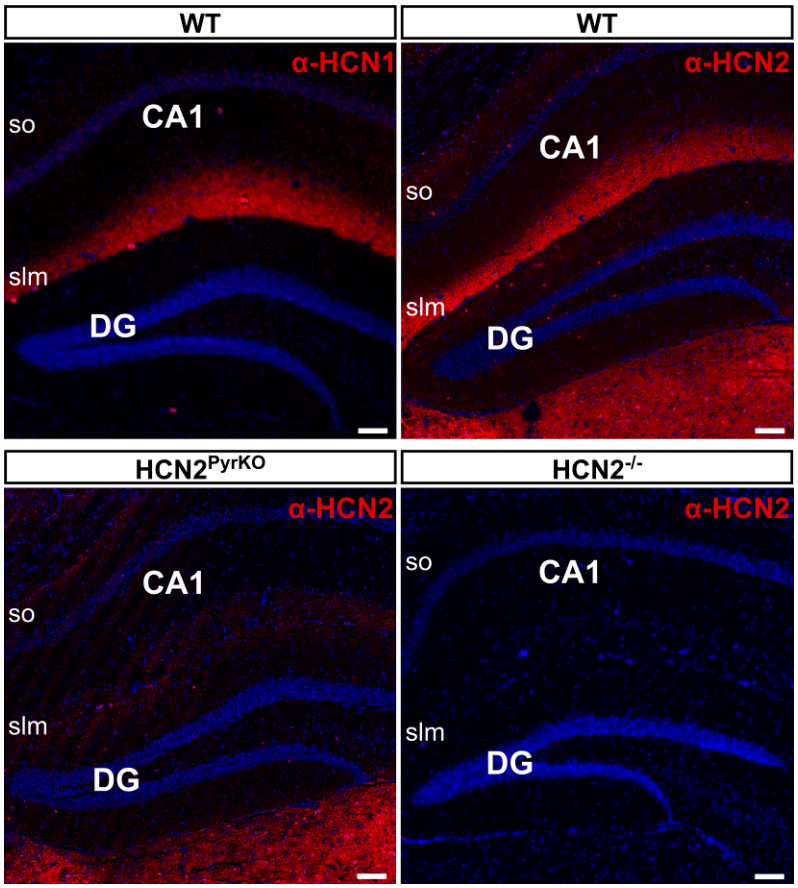


Figure 10: Expression of the HCN1 and HCN2 channel subunits in the hippocampal CA1-region. Immunohistochemistry of coronal brain slices from the genotypes indicated using fluorescently-labeled antibodies (red) against the HCN1 (α-HCN1) and the HCN2 (α-HCN2) channel subunits. Nuclei are visualized by Hoechst staining (blue). Both channels show ribbon-like distribution in the *stratum lacunosum moleculare* (**slm**) corresponding to the distal dendrites of pyramidal cells. High levels of HCN2 immunoreactivity were also detected in thalamic areas ventral to the *dentate gyrus* (**DG**). In the conditional knockout ($HCN2^{PyrKO}$) the HCN2 channel protein is lost in the **slm** revealing residual puncta-shaped immunoreactivity in various hippocampal layers including the *stratum oriens* (**so**), while the thalamic expression remains nearly unchanged. Sections from $HCN2^{-/-}$ mice are included to demonstrate the specificity of the α-HCN2 antibody used. The scale bar corresponds to 100 µm.

Initially, the expression of HCN1 and HCN2 channels in the hippocampus was examined by immunohistochemistry (2.3). As reported previously (cf. Nolan et al., 2004; Notomi and Shigemoto, 2004), the expression of the HCN1 subunit in the

hippocampus is restricted to a distinct, ribbon-shaped region corresponding to the *stratum lacunosum moleculare* (**slm**; Figure 10, upper left). In this area, the direct perforant path (PP) forms synapses to the distal dendrites of CA1 pyramidal cells. Strikingly, the distribution of HCN2 immunoreactivity in the hippocampus of wild type mice reveals a fairly similar pattern (Figure 10, upper right), suggesting a strong overlap in the expression patterns of both HCN channels in distal dendrites of hippocampal pyramidal neurons. In contrast to HCN1, HCN2 was also expressed in thalamic areas (Figure 10, upper right).

Specificity of the antibodies directed against HCN1 and HCN2 was confirmed by the lack of specific staining in brain sections from the respective null mutants (Figure 10, lower right).

In conclusion, the HCN1 and HCN2 subunits show an overlapping distribution in the hippocampus. Based on this finding, one might expect that both channel subunits either serve a similar function in distal dendrites of CA1 pyramidal cells or fulfill similar roles by forming functional heterotetramers.

## *3.2 The pyramidal neuron specific conditional knockout*

Two genetically modified mouse lines were used to elucidate the relevance of the HCN2 channel expressed in hippocampal pyramidal neurons: (*i*) the global knockout mouse $HCN2^{-/-}$ (2.1.2.2), that has been previously described (Ludwig et al., 2003), and (*ii*) the newly generated conditional knockout mouse (2.1.2.3) lacking the HCN2 gene in glutamatergic neurons of the forebrain. PCR analysis (2.1.3.2) of genomic DNA isolated from mice heterozygous for the conditional L2 allele and the Cre transgene (genotype: $HCN2^{+/L2}$; $NEX^{+/Cre}$) demonstrated the conversion of the floxed L2 allele into the HCN2 null allele (L1) in the hippocampus and neocortex showing that recombination was effective (Figure 11A). The

remaining L2 band arises from the presence of genomic DNA from non-pyramidal and non-neuronal cells in the tissue samples. Importantly, no recombination was detected in the thalamus and skeletal muscle used as negative control for the recombination system. Additional evidence demonstrating the efficiency of Cre-mediated recombination was provided by Western blot analysis of CA1 pyramidal cells (2.2) and immunohistochemical analysis (2.3). Immunoblotting of tissue samples from the hippocampus of control and conditional knockout mice (Figure 11B) revealed a strong reduction of a specific band corresponding to the HCN2 protein in the knockout hippocampus, olfactory bulb and cortex, but not in the thalamus. This pattern resembles the expression of Cre in the transgenic Nex-Cre mouse line (Goebbels et al., 2006).

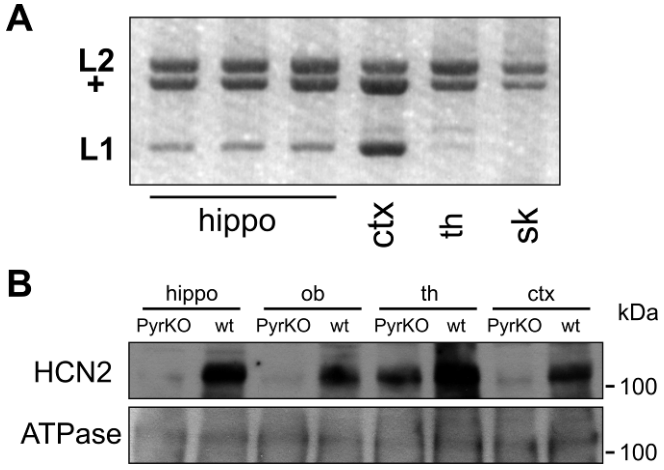


Figure 11: Hippocampal expression of HCN2 is strongly reduced in the conditional knockout ($HCN2^{PyrKO}$). **(A)** PCR analysis of Cre-mediated recombination. Genomic DNA isolated from the indicated tissues was used as a template. All tissue samples were obtained from 6-week-old $HCN2^{PyrCtr}$ mice (genotype: $HCN2^{+/L2}$; $NEX^{+/Cre}$). PCR products amplified from the different HCN2 alleles are indicated (wild type (+), L2 and L1). **(B)** Western Blot analysis of the HCN2 protein expression in various tissues of 8-week-old $HCN2^{PyrCtr}$ and $HCN2^{PyrKO}$ (genotype: $HCN2^{L1/L2}$; $NEX^{+/Cre}$) mice respectively. As loading control, the expression of ATPase was analyzed in the same samples. The blot is representative of three independent experiments. ctx: neocortex; hippo: hippocampus; ob: olfactory bulb; sk: skeletal muscle; th: thalamus.

In line with this, immunoreactivity for the HCN2 channel was not detectable in the hippocampus of sections from the conditional knockout mice (Figure 10, lower left).

Acknowledging the ablation of the HCN2 gene in pyramidal cells, the conditional knockout was referred to as $HCN2^{PyrKO}$ (genotype: $HCN2^{L1/L2}$; $NEX^{+/Cre}$) and the corresponding controls as $HCN2^{PyrCtr}$ (genotype: $HCN2^{+/L2}$; $NEX^{+/Cre}$).

$HCN2^{PyrKO}$ mice did not display the neuronal phenotypes observed in HCN2 null mutants (Ludwig et al., 2003) and exhibited a normal life expectancy. Both mouse lines lack gross anatomical abnormalities in the brain, and the cellular layers in the hippocampus are regularly arranged.

These data demonstrate that there is virtually no expression of the HCN2 protein in pyramidal neurons of the conditional $HCN2^{PyKO}$ mouse. Therefore, the $HCN2^{PyKO}$ mouse represents a valid model to study the postsynaptic effect of HCN2 channels in hippocampal synaptic plasticity.

## *3.3 LTP in the PP is not influenced by HCN2 in CA1 pyramidal cells*

### 3.3.1 LTP is enhanced in the PP of $HCN1^{-/-}$ mice

Mice bearing a knockout of the HCN1 channel in principal neurons of the forebrain show improved learning in the water maze test. This phenotype was reflecting changes in synaptic plasticity, namely elevated long-term potentiation (LTP) in PP inputs to CA1 pyramidal cells (Nolan et al., 2004). As the expression pattern of the HCN2 channel in the hippocampus resembled that of HCN1 to a considerable degree (Figure 10) it was speculated that both proteins serve a similar function in hippocampal synaptic plasticity. Before elucidating this hypothesis, the LTP phenotype of HCN1-deficient mice was reproduced under modified experimental conditions (with intact GABAergic inhibition and using a different tetanus for the stimulation of LTP).

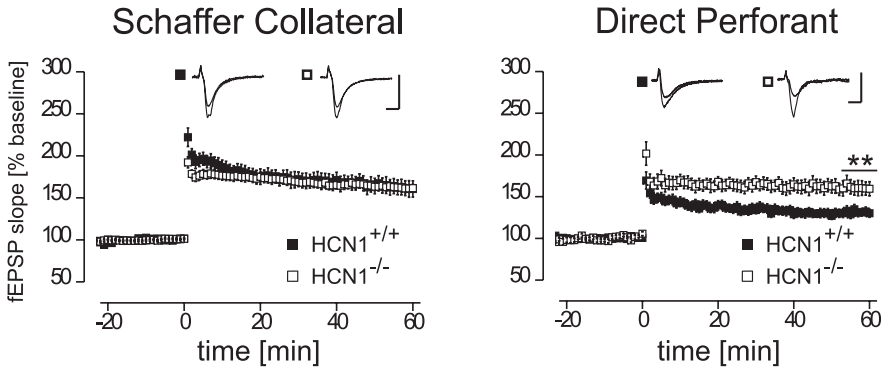


Figure 12: Mutant mice lacking the HCN1 channel ($HCN1^{-/-}$, open squares) show enhanced LTP in the direct perforant (PP, right panels) but not in the Schaffer collateral (SC, left panels) pathway when compared to littermate controls ($HCN1^{+/+}$, filled squares). The scale bar of the representative recordings corresponds to 10 ms and 1 mV.

Figure 12 displays the results of the LTP measurements in the PP and the Schaffer collateral (SC) pathway of $HCN1^{+/+}$ and $HCN1^{-/-}$ mice (2.4.2). The excitatory postsynaptic potential (EPSP) evoked by electric stimulation is recorded as field potential (fEPSP). After registration of the baseline slope of the fEPSP for 20 min, a stimulation at high frequency, the so-called tetanus (4x 0.5 s, 100 Hz) was applied. Tetanic stimulation persistently increased the slope of the fEPSP, the effect commonly referred to as LTP. In the absence of a $GABA_A$ receptor-antagonist and by using a strong tetanic stimulation, a significant increase of LTP ($p<0.01$) was found in the PP of HCN1 null mutants ($HCN1^{-/-}$: 174 ± 8%, n=9 versus $HCN1^{+/+}$: 135 ± 4%, n=8), while it was normal in the SC pathway ($HCN1^{+/+}$: 160 ± 9%, n=6 versus $HCN1^{-/-}$: 161 ± 5%, n=17). These experiments confirmed the phenotype previously reported for HCN1-deficient mice (Nolan et al., 2004) despite important modifications of the experimental conditions.

### 3.3.2 Basal synaptic transmission in HCN mutants is not impaired

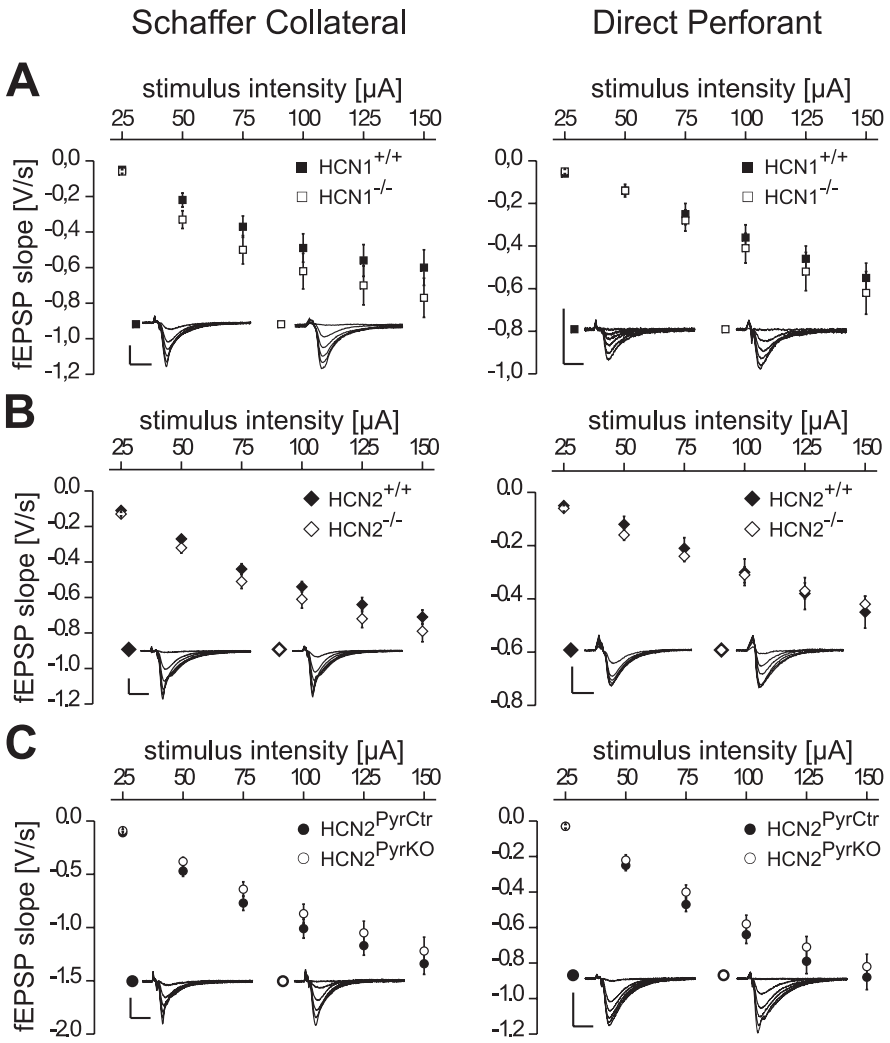


Figure 13: None of the HCN channel mutants displays changes in the I/O relation in either SC (left panels) or PP (right panels) inputs. **(A)** HCN1 knockout mice ($HCN1^{-/-}$, open circles) and their littermate controls ($HCN1^{+/+}$, filled circles). **(B)** Wild type ($HCN2^{+/+}$, filled diamonds) and littermate $HCN2^{-/-}$ mice (open diamonds). **(C)** Conditional HCN2 knockout mice ($HCN2^{PyrKO}$, open circles) and their littermate controls ($HCN2^{PyrCtr}$, filled circles). The scale bars of the representative recordings correspond to 10 ms and 1 mV.

Before exploring the effect of the HCN2 deletion on LTP in the mutant mice, the absence of general defects in synaptic transmission was verified. Possible differences in the fundamental mechanisms of signal transmission caused by genetic modification include for example: (*i*) altered electric propagation of action potentials, (*ii*) changes in presynaptic transmitter release, or (*iii*) variations in

postsynaptic physiology. Any of these faults could influence LTP in a way resembling a phenotype in synaptic plasticity. To rule out any influence of alterations in basal synaptic transmission, the dependency of the fEPSP amplitude on the stimulus intensity (I/O relation) was analyzed for stimulation intensities from 25 µA to 150 µA in the SC and the PP of brain slices from the different mouse lines. In all three mutant strains ($HCN1^{-/-}$: n=19/26 (SC/PP); $HCN2^{-/-}$: n=54/24; and $HCN2^{PyrKO}$: n=21/12) the I/O relation in both synaptic inputs matched (Figure 13) that of the respective littermate controls ($HCN1^{+/+}$: n=23/23 (SC/PP); $HCN2^{+/+}$: n=47/13 ; and $HCN2^{PyrCtr}$: n=34/9).

Another important control parameter of synaptic transmission is the paired-pulse facilitation (PPF) that presumably corresponds to presynaptic function. In this experiment a pair of identical stimuli is applied with a relatively short pause (25-100 ms) resulting in the amplification of the second fEPSP. The PPF is the ratio of the slopes of the second and first fEPSP. Again, the mutant mouse lines ($HCN1^{-/-}$: n=19/26 (SC/PP); $HCN2^{-/-}$: n=54/24; and $HCN2^{PyrKO}$: n=21/12) showed normal PPF in both the SC and perforant path inputs to hippocampal CA1 pyramidal neurons (Figure 14) when compared to littermate controls ($HCN1^{+/+}$: n=23/23 (SC/PP); $HCN2^{+/+}$: n=47/13 ; and $HCN2^{PyrCtr}$: n=34/9).

In conclusion, none of the examined HCN mutants displayed a general defect of synaptic transmission.

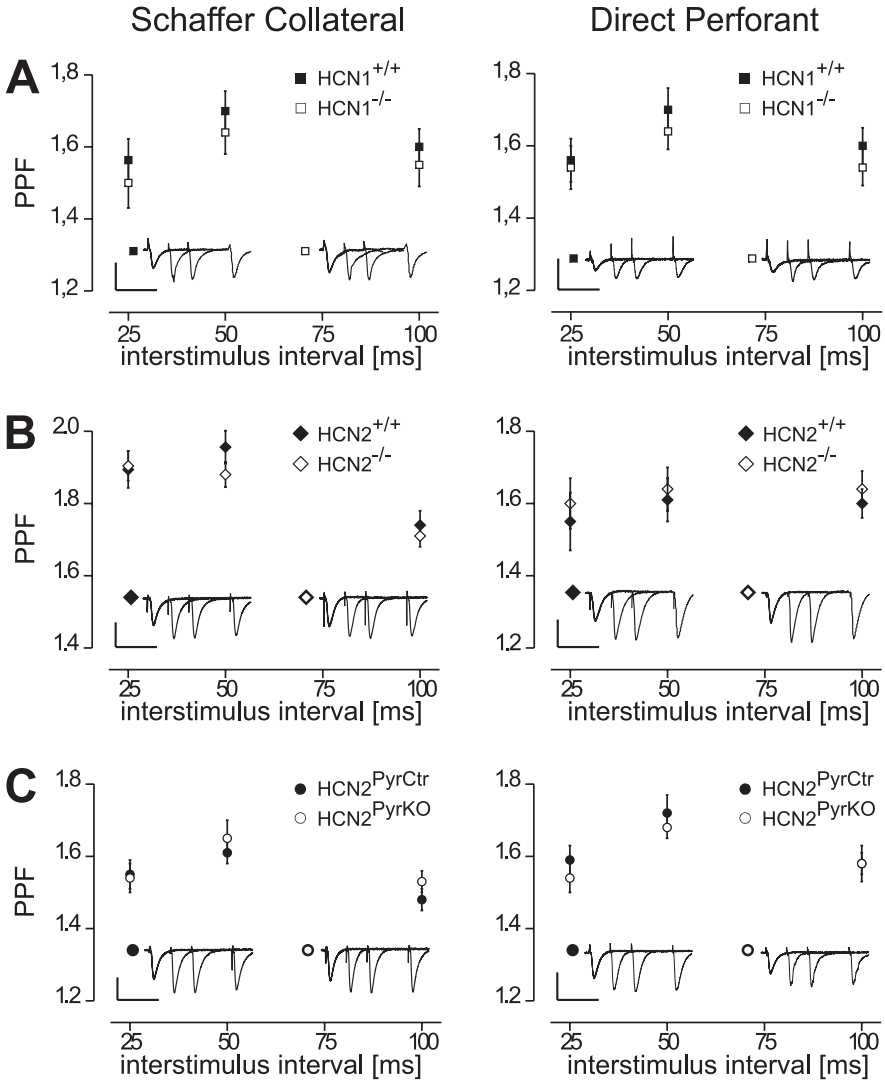


Figure 14: None of the HCN channel mutants displays changes in the paired-pulse facilitation (PPF) in either SC (left panels) or PP (right panels) inputs. **(A)** HCN1 knockout mice ($HCN1^{-/-}$, open circles) and their littermate controls ($HCN1^{+/+}$, filled circles). **(B)** Wild type ($HCN2^{+/+}$, filled diamonds) and littermate $HCN2^{-/-}$ mice (open diamonds). **(C)** Conditional HCN2 knockout mice ($HCN2^{PyrKO}$, open circles) and their littermate controls ($HCN2^{PyrCtr}$, filled circles). The scale bars of the representative recordings correspond to 10 ms and 1 mV.

### 3.3.3 LTP is enhanced in the PP of $HCN2^{-/-}$ but not of $HCN2^{PyrKO}$

So far, the performed experiments demonstrated that basal synaptic transmission is unaltered in the mouse models with genetically inactivated HCN channels and that any changes observed in hippocampal LTP would indeed reflect the influence of the mutation on synaptic plasticity (3.3.2). Additionally, the LTP phenotype of HCN1 null mutants (Nolan et al., 2004) was reproduced under the experimental

conditions of this study (3.3.1). Next, LTP was examined under these conditions in mice homozygous for the general HCN2 null mutation ($HCN2^{-/-}$). Resembling the findings in HCN1-deficient mice, $HCN2^{-/-}$ mice showed the same LTP level in the SC pathway (Figure 15A) as their controls ($HCN2^{-/-}$: 144 ± 4%, n=16 versus $HCN2^{+/+}$: 149 ± 6%, n=13). In the PP however, LTP of mice lacking the HCN2 channel was significantly ($p<0.01$) increased in comparison to controls ($HCN2^{-/-}$: 163 ± 4%, n=11 versus $HCN2^{+/+}$: 131 ± 6%, n=11).

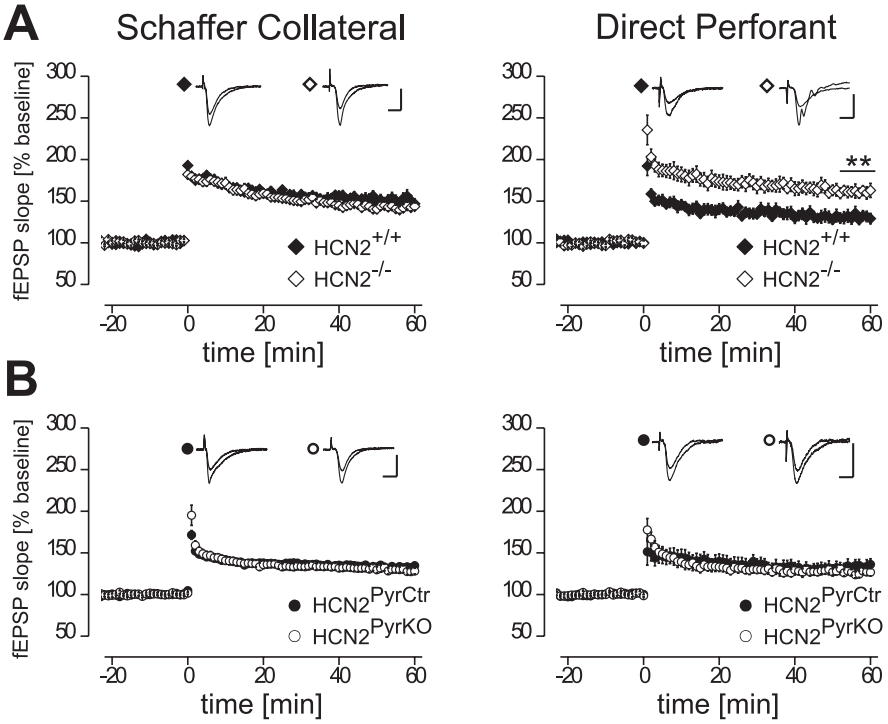


Figure 15: LTP in the Schaffer collateral (SC, left panels) and direct perforant path (PP, right panels) inputs of mutant mice lacking the HCN2 channel. Enhanced LTP was observed in the PP of HCN2 null mutants ($HCN2^{-/-}$), but not in the conditional knockout mice lacking the HCN2 in pyramidal neurons ($HCN2^{PyrKO}$). **(A)** $HCN2^{+/+}$ (filled diamonds) and littermate $HCN2^{-/-}$ mice (open diamonds). **(B)** $HCN2^{PyrKO}$ (open circles) and littermate $HCN2^{PyrCtr}$ (filled circles). The scale bars of the representative recordings correspond to 10 ms and 1 mV.

Due to their maximal levels of expression in the distal dendrites of CA1 pyramidal cells, HCN1 channels constrain synaptic plasticity in the PP by damping incoming EPSPs at these postsynaptic sites most effectively (Magee, 1998; Nolan et al., 2004). So far, the findings are in line with the new idea that HCN2 channels serve

a similar function for hippocampal synaptic transmission. To verify this assumption, hippocampal LTP of $HCN2^{PyrKO}$ mice lacking the HCN2 gene in postsynaptic CA1 pyramidal neurons was compared to the corresponding controls ($HCN2^{PyrCtr}$). As anticipated, LTP in the SC was not different (Figure 15B, left panel) between these genotypes ($HCN2^{PyrCtr}$: 135 ± 4%, n=18 versus $HCN2^{PyrKO}$: 130 ± 4%, n=19). Interestingly, and in contrast to mice with a forebrain-specific deletion of the HCN1 channel, $HCN2^{PyrKO}$ mice also showed no increased LTP in the PP (Figure 15B, right panel). Virtually the same amount of LTP was observed in inputs to the distal dendrites of CA1 pyramidal cells in $HCN2^{PyrCtr}$ (132 ± 7%, n=9) and $HCN2^{PyrKO}$ (127 ± 4%, n=13) mice. As already discussed, a general defect of hippocampal synaptic transmission in these mice could not account for this finding (3.3.2).

## *3.4 HCN2 is expressed in somatostatin-positive stratum oriens interneurons*

The lack of enhanced LTP in $HCN2^{PyrKO}$ mice may result from insufficient recombination efficiency in CA1 pyramidal cells of this mouse model. However, this possibility could be ruled out by immunohistochemical analysis of the hippocampus (2.3) since a massive reduction of HCN2 immunoreactivity in the hippocampus of $HCN2^{PyrKO}$ mice was detected (Figure 10, lower left). Nevertheless, the HCN2 immunoreactivity was completely absent only in sections from $HCN2^{-/-}$ mice, whereas a weak residual staining was still present in the hippocampus of the $HCN2^{PyrKO}$ mice (Figure 10). Remarkably, the staining pattern differed from the homogeneous distribution of the channel in the **so** observed in the wild type. The residual immunoreactivity was restricted to individual spots throughout the *strata oriens*, *radiatum* and *lacunosum moleculare* coinciding with the localization of local inhibitory interneurons (Freund and Buzsaki, 1996). It was

shown that the HCN2$^{PyrKO}$ mice lack Cre expression in GABAergic interneurons (Goebbels et al., 2006). This implied that HCN2$^{PyrKO}$ mice did not show the phenotype observed in HCN2 null mutants because it resulted primarily from a function of HCN2 channels in hippocampal inhibitory interneurons. Based on this, it was hypothesized that the HCN2 channel facilitates output from local interneurons onto distal dendrites of CA1 pyramidal neurons.

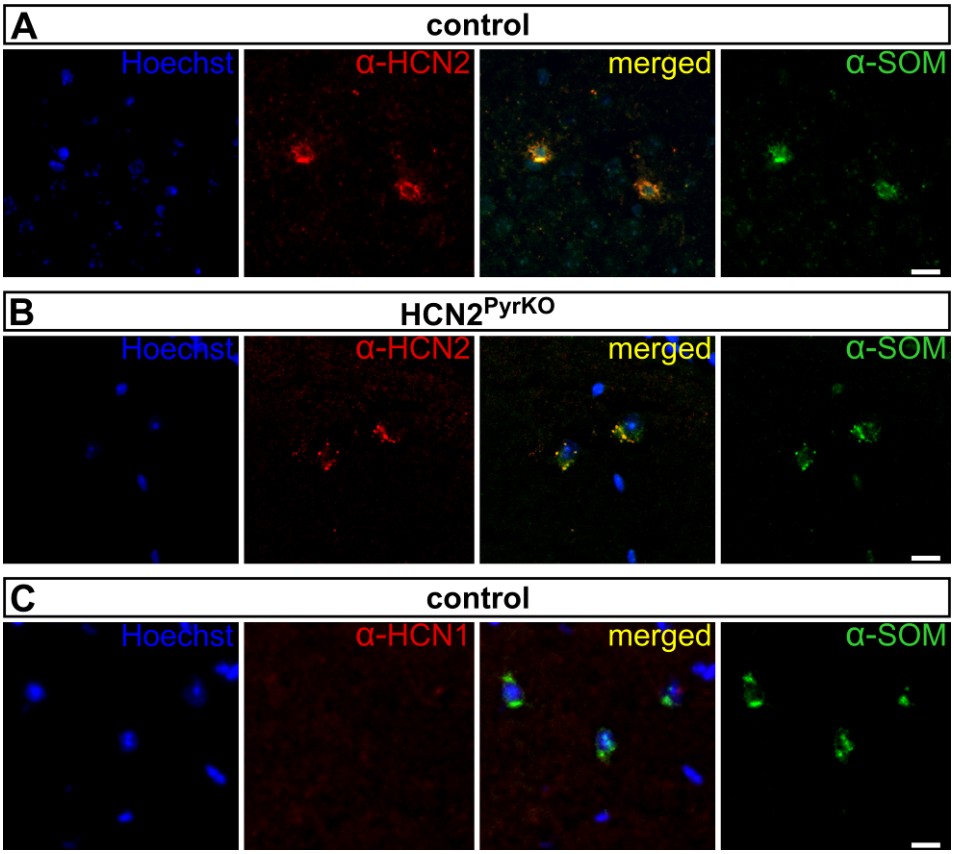


Figure 16: High magnification of confocal fluorescence images from interneurons in the *stratum oriens* (**so**) of WT and HCN2$^{PyrKO}$ mice. **(A-B)** The soma of interneurons in the **so** of WT and HCN2$^{PyrKO}$ mice were co-stained by antibodies directed against HCN2 (α-HCN2, red) and somatostatin (α-SOM, green). Merged images illustrate overlapping expression (yellow). Nuclei were counterstained using the nuclear marker Hoechst (blue). **(C)** No immunohistochemical labeling of the HCN1 channel (α-HCN1, red) is detectable in the soma of somatostatin-positive **so** interneurons. The scale bar corresponds to 10 µm.

Among the numerous types of dendrite-targeting interneurons (Klausberger, 2009), oriens-lacunosum moleculare (O-LM) cells exhibit special features related to synaptic transmission in the PP (Blasco-Ibanez and Freund, 1995; Katona et al.,

1999). Located in the **so**, they receive excitatory inputs from CA1 pyramidal cells and, in turn, provide inhibitory feedback at distal dendrites in the **slm**. Double immunostainings were performed to test if HCN2 channels were expressed in interneurons of the *stratum oriens*. O-LM interneurons were identified by their expression of the neuropeptide somatostatin which is commonly used as a specific marker for these cells (Losonczy et al., 2002; Somogyi and Klausberger, 2005). Indeed, HCN2 immunoreactivity was detected in the soma of somatostatin-positive cells in the **so** of wild type animals (Figure 16A). More importantly, the same co-expression was also observed in cells located in the **so** of $HCN2^{PyrKO}$ animals (Figure 16B) further reinforcing the view that local interneurons in these mutants still express the HCN2 channel. In contrast, no HCN1 immunoreactivity was detected in the soma of somatostatin-positive hippocampal interneurons (Figure 16C). This finding does not rule out the expression of HCN1 channels in O-LM cells at loci different from the soma. However, it supports the view that HCN2 and HCN1 serve different functions in O-LM cells, as well as they restrict LTP in the PP by different mechanisms.

## *3.5 $HCN2^{-/-}$ mice show impaired inhibition of the PP*

### 3.5.1 Disinhibition enhances LTP in the PP of $HCN2^{+/+}$ but not $HCN2^{-/-}$

The increased LTP in the PP of HCN2 null mutants may reflect a function of HCN2 channels in local interneurons, inhibiting the distal dendrites of CA1 pyramidal neurons. The loss of the HCN2 channel diminishes the action of these interneurons thereby enhancing LTP. To test this hypothesis, the effect of disinhibition on LTP in the PP of wild type and $HCN2^{-/-}$ mice was simulated using the $GABA_A$ receptor-antagonist picrotoxin (PiTX). Fittingly, PiTX (50 µM) increased

LTP in PP inputs of the wild type about 25% ($HCN2^{+/+}$ with PiTX: 161 ± 8%, n=14), whereas it had no effect on LTP observed in the PP of HCN2 mutants ($HCN2^{-/-}$ with PiTX: 159 ± 12%, n=8) (Figure 17). Obviously, inhibition of PP transmission in $HCN2^{-/-}$ is impaired, as PiTX does not enhance the amount of LTP recorded in this input. In fact, blockade of the $GABA_A$ receptor-mediated synaptic transmission abolished the difference in LTP between both genotypes that was observed when inhibitiory mechanisms were intact.

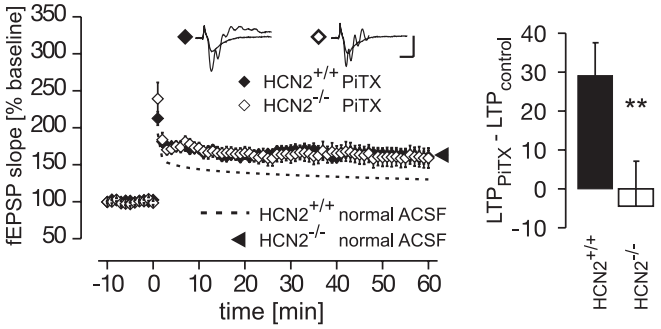


Figure 17: Wild type ($HCN2^{+/+}$, filled diamonds) mice and HCN2 null mutants ($HCN2^{-/-}$, open diamonds) show equivalent LTP in the direct perforant pathway under conditions of disinhibition. The $GABA_A$ receptor-antagonist picrotoxin (PiTX, 50 µM) was present in all experiments. LTP in the absence of PiTX is indicated by the dotted line ($HCN2^{+/+}$) and the arrowhead ($HCN2^{-/-}$). Scale bars correspond to 10 ms, 1 mV. The right panel illustrates the difference of LTP measured with or without PiTX present ($LTP_{PiTX}$-$LTP_{control}$) for both genotypes.

### 3.5.2 Basal inhibition of the PP is impaired in $HCN2^{-/-}$ mice

Measuring LTP in $HCN2^{-/-}$ under conditions of disinhibition revealed that PP LTP in these mice was not influenced by GABAergic transmission (3.5.1). Nevertheless, it is still unknown whether the deletion of the HCN2 gene also reduces the functional inhibition of excitatory transmission under basal conditions independent of synaptic plasticity. To test this, fEPSPs were evoked every 15 s in glutamatergic inputs to CA1 pyramidal cells of wild type and $HCN2^{-/-}$ mice. As expected, washing PiTX into the bath solution increased the slope of fEPSPs measured in the SC pathway of $HCN2^{+/+}$ (132 ± 4%, n=13) and $HCN2^{-/-}$ (130 ± 5%, n=8) to a similar extent

(Figure 18A). In the PP however, PiTX increased the slope of fEPSPs in $HCN2^{+/+}$ mice (123 ± 3%, n=33) while it failed to do so in littermate $HCN2^{-/-}$ mice (99 ± 2%, n=11, $p<0.001$). Interestingly, PiTX did also increase the fEPSP slope (Figure 18B) in the SC of $HCN1^{-/-}$ mice (SC: 137 ± 6%, n=9; PP: 109 ± 4%, n=21), while the effect in the PP was significantly ($p<0.01$) less pronounced than in the wild type. In contrast to $HCN2^{-/-}$ mice, the fEPSP slope in the PP of $HCN1^{-/-}$ increased after the application of PiTX.

Taken together with the fact that PiTX failed to enhance LTP in the PP, these data suggested a defect of inhibitory transmission under basal conditions and during high-frequency stimulation in $HCN2^{-/-}$ mice. Astonishingly, this impairment was restricted to the glutamatergic inputs connecting to the distal dendrites of CA1 pyramidal cells. Additionally, also the HCN1 channel seems to play a role in the basal inhibitory activity of certain hippocampal inhibitory interneurons.

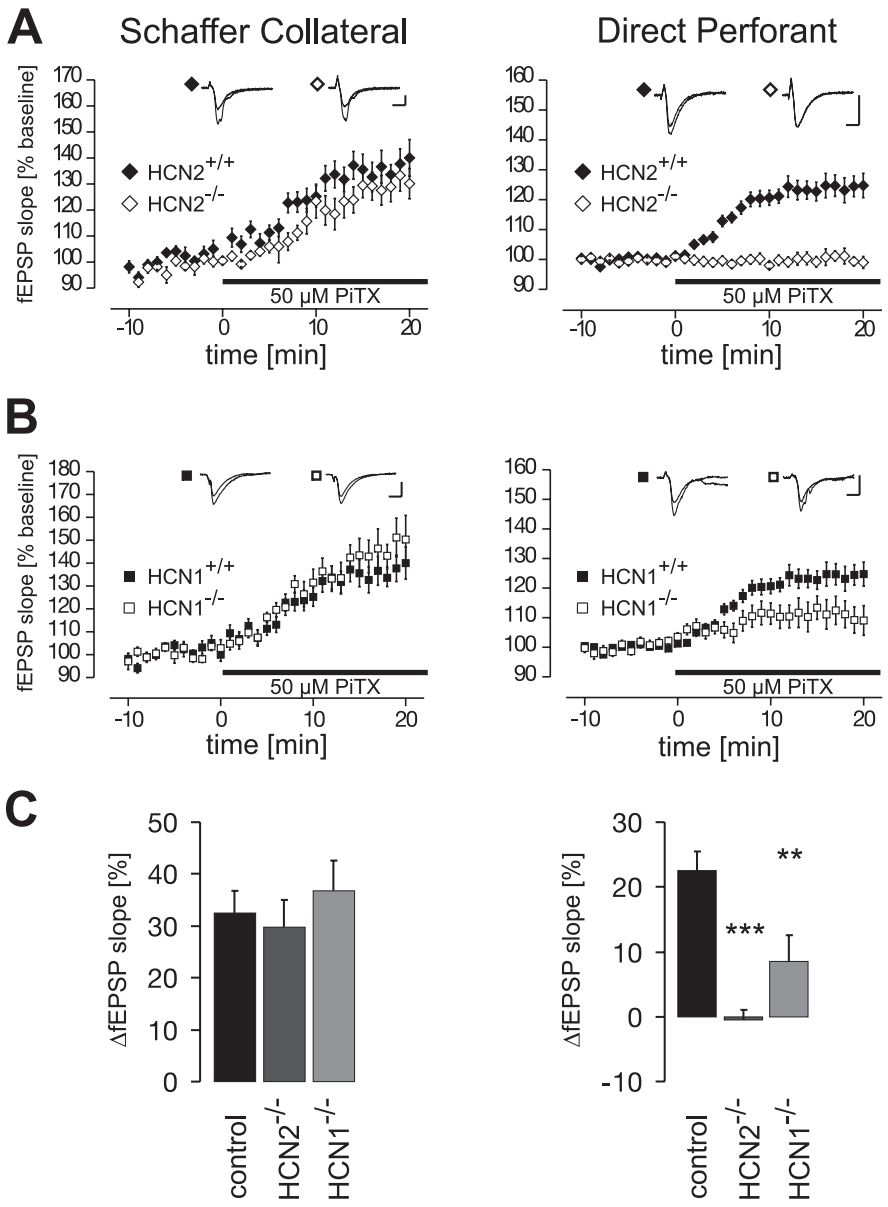


Figure 18: The HCN2 channel is critical for the inhibition of basal synaptic transmission in the PP (right panels), but not the SC pathway (left panels). Basal synaptic transmission was recorded for about 10 min in normal aCSF before washing picrotoxin (PiTX, 50 µM). **(A)** In SC inputs, the PiTX-induced rise of the fEPSP slope was not different between wild type ($HCN2^{+/+}$, filled diamonds) and littermate HCN2 null mutants ($HCN2^{-/-}$, open diamonds). However, PiTX increased the fEPSP slope in the PP of $HCN2^{+/+}$ while failing to do so in $HCN2^{-/-}$ mice. **(B)** $HCN1^{-/-}$ animals (open squares) showed the same increase of fEPSP slope in SC inputs as $HCN1^{+/+}$ (filled squares). In the PP however, PiTX induced only a moderate increase of the fEPSP slope in $HCN1^{-/-}$ compared to the littermate $HCN1^{+/+}$. **(C)** The panels illustrate the mean changes of the fEPSP slope following treatment with PiTX for both pathways. The controls from both HCN1 and HCN2 experiments were pooled. The scale bar of the representative recordings corresponds to 10 ms and 1 mV.

### 3.5.3 HCN2 increases the frequency of sIPSCs in CA1 pyramidal cells

A more direct approach to monitor the function of local GABAergic interneurons is the recording of spontaneous inhibitory postsynaptic currents (sIPSC) in CA1 pyramidal cells. sIPSCs were measured while blocking all excitatory transmission (see 2.4.3.2). All remaining currents under these conditions stem from the activation of $GABA_A$ receptors. Therefore, the frequency and amplitude of sIPSC measured in CA1 pyramidal cells from wild type and $HCN2^{-/-}$ mice was analyzed (Figure 19). Results of the control animals from all tested mouse lines did not differ and were pooled as a single control group. Reinforcing the view that the HCN2 channel is critical for the function of local interneurons, the frequency of sIPSCs in CA1 pyramidal cells of $HCN2^{-/-}$ mice (2.1 ± 0.2 Hz, n=6) was significantly ($p<0.05$) reduced compared to controls (4.0 ± 0.5 Hz, n=8; Figure 19B, left panel). In addition, the application of the HCN channel inhibitor zatebradine led to a significant ($p<0.01$) reduction in the frequency of control animals (1.7 ± 0.3 Hz, n=8) but not in $HCN2^{-/-}$ (1.3 ± 0.1 Hz, n=6) mice (Figure 19B, left panel). Further reinforcing the relevance of the HCN2 channel, $HCN1^{-/-}$ mice displayed only a tendential reduction of the basal sIPSC frequency (2.9 ± 0.5 Hz, n=6) in comparison to littermate controls while zatebradine evoked a significant ($p<0.05$) decrease (1.5 ± 0.2 Hz, n=6). After these findings, it is not surprising that the frequency of sIPSCs in CA1 pyramidal neurons of HCN-DKO was also significantly ($p<0.01$) reduced (1.1 0± 0.2 Hz, n=5) under basal conditions but virtually not affected by the application of zatebradin (0.7 ± 0.3 Hz, n=5).

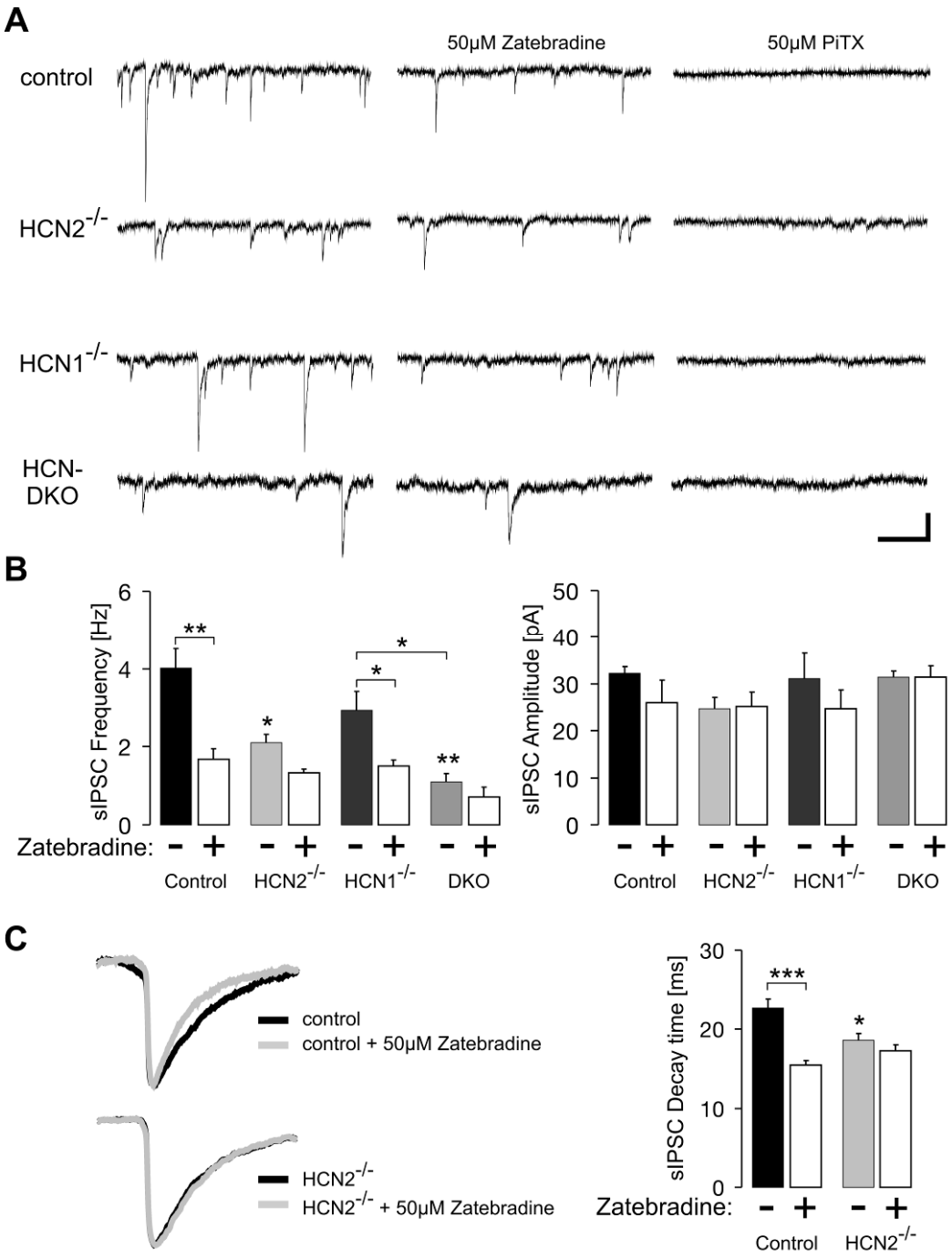


Figure 19: The HCN2 channel supports spontaneous inhibitory currents (sIPSC) in CA1 pyramdial cells. **(A)** Representative voltage-clamp recordings of sIPSC in CA1 pyramidal neurons of wild type (control), $HCN2^{-/-}$, $HCN1^{-/-}$, and HCN-DKO mice. The $GABA_A$ inhibitor picrotoxin (PiTX) serves as internal control verifying GABAergic currents by completely abolishing all sIPSC. Scale bar: 20 pA, 200 ms. **(B)** Mean values for frequency (left panel) and amplitude (right panel) of sIPSCs before and after adding the HCN channel blocker zatebradine. **(C)** Average of 200 normalized synaptic events before (black traces) and after the application of zatebradine (grey traces) in control and $HCN2^{-/-}$ mice (left panel). Mean sIPSC decay times before and after the addition of zatebradine (right panel).

No differences (Figure 19B, right panel) were found comparing the mean amplitudes of sIPSCs in all different mouse lines under basal conditions (control: 32 ± 2 pA n=8; $HCN2^{-/-}$: 25 ± 2 pA, n=6; $HCN1^{-/-}$: 31 ± 5 pA, n= 6; HCN-DKO: 31 ± 1 pA, n=5) and after the application of zatebradine (wild type: 26 ± 5 pA, n=8; $HCN2^{-/-}$: 25 ± 3 pA, n=6, $HCN1^{-/-}$: 25 ± 4 pA, n=6; HCN-DKO: 31 ± 2 pA, n=5).

Additionally, the mean decay time constant of sIPSC in $HCN2^{-/-}$ animals (18.6 ± 0.9 ms, n=6) was significantly ($p<0.05$) reduced compared to littermate controls (22.7 ± 1.2 ms, n=8; Figure 19C). The application of zatebradine reduced the decay time significantly ($p<0.05$) in wild type (15.5 ± 0.6 ms, n=8) but not in $HCN2^{-/-}$ mice (17.3 ± 0.7 ms, n=6).

The application of PiTX completely abolished sIPSC activity in all genotypes, thereby documenting that all currents measured in these experiments are indeed conducted by $GABA_A$ receptors. Confirming a previous report (Lupica et al., 2001), these findings indicate that spontaneous activity of local inhibitory interneurons targeting CA1 pyramidal cells critically depends on the function of HCN1 and HCN2 channels.

### 3.5.4 O-LM cells contribute to sIPSCs in CA1 pyramidal cells

The HCN channel blocker zatebradine reduces the frequency of sIPSCs recorded in CA1 pyramidal cells (3.5.3). However, the identity of the presynaptic GABAergic interneurons responsible for the observed reduction in sIPSC frequency remains unresolved. Another marker protein for O-LM interneurons (Ferraguti et al., 2004) is the metabotropic glutamate receptor subtype 1 (mGluR1). mGluR1 was shown to simultaneously increase the activity of O-LM interneurons and the frequency of sIPSCs in pyramidal cells (Taketo and Matsuda, 2010). As expected, dihydroxyphenylglycine (DHPG), a selective mGluR1 agonist significantly ($p<0.001$)

increases the frequency of sIPSC in pyramidal cells of wild type animals (basal: 4.9 ± 0.7 Hz, n=12; DHPG: 12.2 ± 1.5 Hz, n=12; Figure 20). Analog to the experiments using zatebradine (3.5.3), DHPG did not influence the mean sIPSC amplitude (basal: 35.5 ± 3.6 pA, n=12; DHPG: 33.7 ± 2.3 pA, n=8). DHPG did also increase the sIPSC frequency in $HCN2^{-/-}$ mice, although on a lower basal level (data not shown). However, the stimulation of the O-LM marker mGluR1 with its agonist DHPG led to an increase in the sIPSC frequency recorded from hippocampal pyramidal neurons indicating the involvement of O-LM interneurons in the generation of sIPSC in CA1 pyramidal cells.

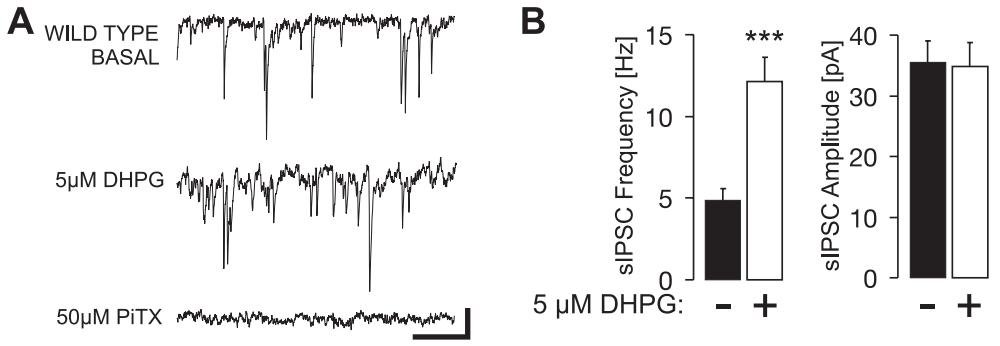


Figure 20: The metabotropic glutamate receptor subtype 1 agonist *S*-(3,5)-dihydroxyphenylglycin (DHPG) stimulates spontaneous inhibitory currents (sIPSC) in CA1 pyramidal cells. (A) Representative voltage-clamp recordings of sIPSCs in CA1 pyramidal neurons of wild type mice. The $GABA_A$ inhibitor picrotoxin (PiTX) serves as internal control for the GABAergic identity of the observed currents by completely abolishing all sIPSCs. Scale bar corresponds to 20 pA and 200 ms. **(B)** Mean values for frequency (left panel) and amplitude (right panel) of sIPSCs before and after the application of DHPG.

## *3.6 Electrophysiological properties of O-LM cells in HCN mutants*

### 3.6.1 Identification of O-LM cells

As indicated by immunohistochemistry (3.4) and the DHPG-sensitivity of sIPSC in pyramidal cells (3.5.4), the function of HCN2 in O-LM interneurons is potentially responsible for the suppression of LTP in the PP. To further verify this assumption

on a functional level, whole-cell patch-clamp experiments (2.4.3) were performed on O-LM cells, which represent the major portion of **so** interneurons (cf. Maccaferri, 2005). The cells were visually identified by their location within the **so** and their (Figure 21) characteristic horizontal dendrites (Maccaferri and Lacaille, 2003). Additionally, the characteristic electrophysiological properties of the cells helped to identify them (Lawrence et al., 2006; Minneci et al., 2007; Klausberger, 2009). In current-clamp mode, O-LM interneurons exhibit a fast, slightly adapting spiking pattern upon injection of a depolarizing current. Upon hyperpolarization, a pronounced depolarizing sag appears, that is completely abolished by the HCN channel inhibitor zatebradine (Figure 23A). Biocytin (see 2.4.3.2) was added to the intracellular solution in a number of experiments. Subsequently performed post-hoc staining and morphological examination of the respective interneurons (Figure 21B) positively confirmed their identity as O-LM cells.

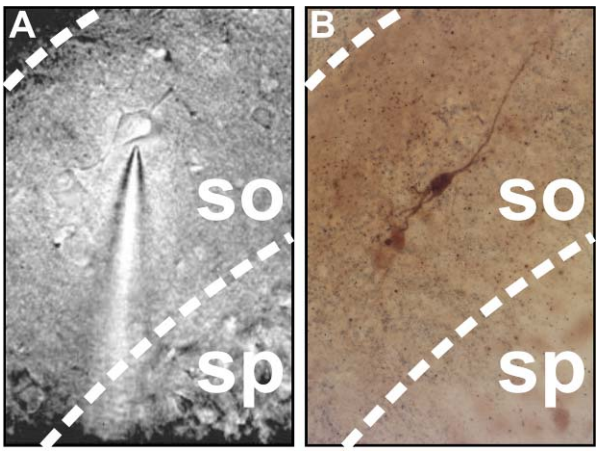


Figure 21: Visual identification of O-LM interneurons. **(A) so** interneuron with horizontal dendrites. Image taken under the microscope used for patch-clamp experiments. **(B)** Post-hoc staining of a biocytin-filled interneuron reveals part of its dendritic tree. The dendrites of the visualized neuron extend horizontally in the *stratum oriens* (**so**). The axon proceeding in the direction of the *stratum pyramidale* (**sp**) is not visible.

### 3.6.2 $I_h$ currents in O-LM cells are mediated by HCN1 and HCN2

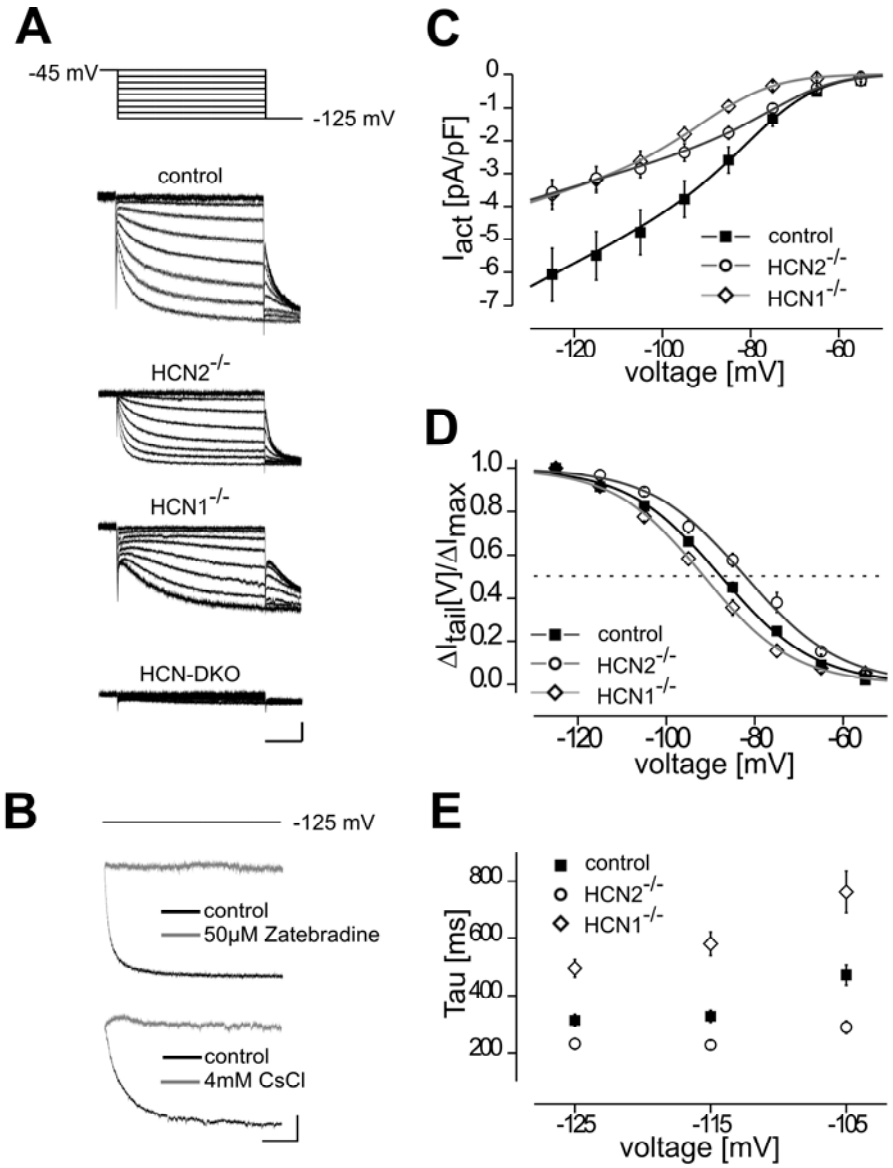


Figure 22: The HCN2 channel subunit mediates a major portion of $I_h$ currents in O-LM interneurons. **(A)** Representative whole-cell voltage-clamp recordings of $I_h$ currents in O-LM cells (lower panels) of 2-week-old wild type (control), $HCN2^{-/-}$, $HCN1^{-/-}$ and double mutant mice lacking both subunits (HCN-DKO). The current density in O-LM cells of $HCN2^{-/-}$ mice is decreased. No $I_h$ currents were detected in HCN-DKO mice at physiological membrane potentials. Scale bars correspond to 500 ms and 200 pA. **(B)** Hyperpolarization-activated membrane currents in O-LM cells are sensitive to blockers of $I_h$ currents. Shown are currents measured at -125 mV in the absence (control, back traces) and in the presence of 4 mM cesium chloride (Cs) and 50 µM zatebradine (gray traces). Scale bars correspond to 500 ms and 200 pA. **(C)** Voltage relationship of the normalized slowly activating current ($I_{act}$) evoked by hyperpolarizing voltage-clamp steps. Instantaneous currents were not taken into account. Smooth curves represent the fit of $I_{act}$ (see 2.4.3.1) **(D)** Dependency of the mean amplitude of the tail current elicited at -125 mV upon test potential (for details see 2.4.3.1). **(E)** Activation kinetics of $I_h$ currents in O-LM cells estimated by a single exponential fit.

To examine the contribution of the HCN2 subunit to $I_h$ currents in O-LM cells, the densities of $I_h$ (2.4.3.1) currents in $HCN1^{-/-}$ and $HCN2^{-/-}$ mice were compared with that in corresponding control animals ($HCN1^{+/+}$ and $HCN2^{+/+}$). There was no difference between $HCN1^{+/+}$ and $HCN2^{+/+}$ mice in terms of $I_h$ currents allowing the combination of both lines to a common control group. Currents were evoked by 2 s hyperpolarizing voltage-clamp steps applied from a holding potential of -45 mV in -10 mV increments and followed by a final voltage-clamp step to -125 mV (Figure 22A, top panel).

Hyperpolarization-activated currents in wild type cells were sensitive to $I_h$ blockers such as cesium and zatebradine (Figure 22B). Remarkably, O-LM cells from $HCN2^{-/-}$ mice (-3.3 ± 0.4 pA/pF, n=20) displayed a significantly ($p<0.01$) decreased normalized $I_h$ current density following a hyperpolarizing voltage-clamp step to -125 mV when compared to controls (-6.0 ± 0.7 pA/pF, n=35). This decrease amounted to approximately 50% (Figure 22A and Figure 22C). The density of $I_h$ currents in O-LM cells from $HCN1^{-/-}$ mice (3.6 ± 0.4 pA/pF, n=22) was also significantly ($p<0.05$) reduced. In animals carrying combined null mutations for the HCN1 and HCN2 channel subunit, no considerable currents were measurable at a membrane potential of -125 mV (Figure 22A). Fitting the curves representing the current-voltage relationships (Figure 22C) for the current fraction activating during hyperpolarizing voltage-clamp steps yielded corresponding relative conductances ($G_{rel}$; for details see 2.4.3.1) of 2.10 ± 0.02 nS (control, n=35), 1.33 ± 0.11 nS ($HCN1^{-/-}$, n=22, $p<0.01$), 1.30 ± 0.15 nS ($HCN2^{-/-}$, n=20, $p<0.05$) and 0.26 ± 0.07 nS (HCN-DKO, n=13, $p<0.001$). Half-maximal activation of $I_h$ currents (Figure 22D) in control animals were estimated as -85.0 ± 0.7 mV (n=35). $I_h$ currents in $HCN2^{-/-}$ (-81.3 ± 1.3 mV, n=20) activated at significantly ($p<0.01$) more positive membrane potentials, comparable to isolated HCN1 channels, whereas $I_h$ currents

of HCN1$^{-/-}$ animals (-90.4 ± 1.2 mV, n=22) needed significantly ($p<0.001$) stronger membrane hyperpolarization to activate, as it is described for the HCN2 channel (Ludwig et al., 1998). Remarkably, remaining $I_h$ currents in HCN2$^{-/-}$ activated much faster than those of the control (Figure 22A), suggesting that the $I_h$ current in O-LM cells lacking the HCN2 channel is composed of rapidly activating HCN1 channels. On the other hand, the remaining $I_h$ currents in O-LM cells from HCN1$^{-/-}$ mice activated much slower, resembling HCN2 channel mediated currents that were recorded in heterologous expression systems (Baruscotti et al., 2005). At a test potential of -125 mV, $I_h$ currents activated (Figure 22E) with a time constant of 314 ± 21 ms (control), 232 ± 19 ms (HCN2$^{-/-}$, $p<0.05$) and 494 ± 31 ms (HCN1$^{-/-}$, $p<0.001$).

All these findings taken together strongly suggest that the HCN1 and HCN2 subunits contribute to $I_h$ currents in O-LM interneurons. Since no residual $I_h$ currents (Figure 22A) were detected at physiological membrane potentials in the double-knockout (HCN-DKO), the contribution of HCN3 and HCN4 subunits could be neglected.

### 3.6.3 HCN channels modulate the resting membrane potential in O-LM interneurons

Additional current-clamp measurements were performed in O-LM cells from the gene-targeted HCN mutants (Figure 23). In line with the assumption that HCN channels show a certain open probability at resting membrane potential (RMP) O-LM cells of HCN2$^{-/-}$ mice were significantly ($p<0.01$) hyperpolarized compared to control cells at rest (RPM control: -60.7 ± 0.4 mV, n=32 versus RPM HCN2$^{-/-}$: -63.2 ± 0.8 mV, n=21). In analogy, the RMP of O-LM cells from HCN1$^{-/-}$ was hyperpolarized ($p<0.001$) (-65.1 ± 1 mV, n=27) while the RMP of HCN double

knockout mice (HCN-DKO, data not shown) was even more negative (-66.7 ± 1.3 mV, n=14). The deletion of the HCN2 gene had no effect on the threshold potential for action potential firing (Thr) in O-LM cells (controls: -43.1 ± 0.9 mV, n=21 versus $HCN2^{-/-}$: -43.8 ± 0.7 mV, n=21). This is indicative for a reduced excitability of O-LM cells in $HCN2^{-/-}$ mice, since eliciting action potentials in these cells requires stronger depolarization because the dilated voltage gap between RMP and Thr needs to be bridged. The Thr potential of O-LM cells from $HCN1^{-/-}$ (-43.1 ± 0.6 mV, n=24) and HCN-DKO mice (-42.0 ± 0.9 mV, n= 10) was as well unaffected.

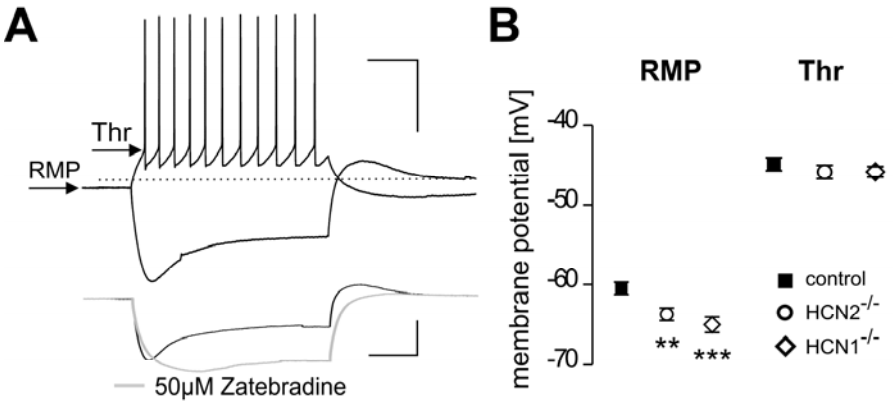


Figure 23: The HCN2 channel regulates resting membrane potential (RMP) and spontaneous activity of O-LM interneurons. Membrane potential recordings were performed in O-LM cells of 2-week-old wild type (control), $HCN2^{-/-}$ and $HCN1^{-/-}$ mice using the whole-cell current-clamp configuration. **(A)** Typical response of O-LM cells from control animals to injection of depolarizing or hyperpolarizing current pulses. RMP was measured with zero current injected. Depolarization beyond a threshold potential (Thr) evoked a weakly accommodating train of action potentials followed by slow afterhyperpolarization. The prominent depolarizing voltage sag present upon hyperpolarization (lower panel, black trace) was eliminated by the application of the $I_h$ current blocker zatebradine (50 µM, gray trace). Scale bars correspond to 500 ms and 50 mV. **(B)** RMP in $HCN2^{-/-}$ and $HCN1^{-/-}$ is significantly reduced in comparison to control, while there is no difference in Thr.

On the other hand, an enhanced excitability of O-LM cells in response to incoming EPSP was detected. The input resistance measured in response to small negative and positive (10-50 pA) current steps was significantly increased in $HCN2^{-/-}$ (284.7 ± 17.7 MΩ, n=17, $p<0.001$) and $HCN1^{-/-}$ mice (259.7 ± 13.6 MΩ, n=23 , $p<0.05$) in

comparison to control animals (227.0 ± 9.9 MΩ, n=36). The input resistance in O-LM cells of HCN-DKO mice was boosted to extreme 1737.7 ± 183.4 MΩ (n=14). These data again strengthen the assumption that HCN1 and HCN2 are the dominant HCN channel subunits in O-LM cells. Additionally, both channels modulate the RMP and the input resistance of O-LM interneurons indicating a function in setting the activity level of these cells.

### 3.6.4 Spontaneous activity in O-LM interneurons of HCN2$^{-/-}$ is not affected by zatebradine

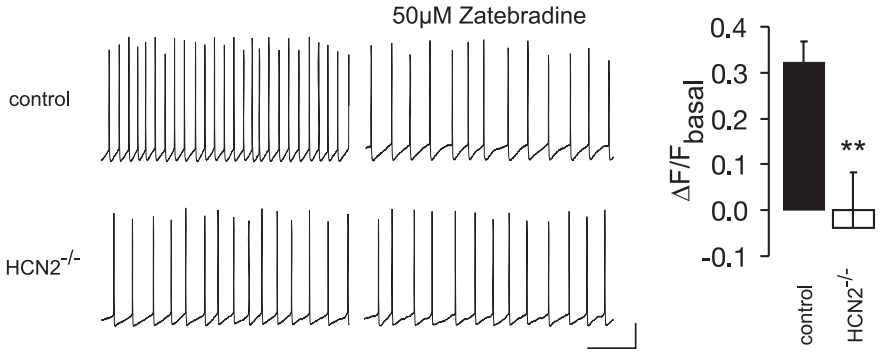


Figure 24: Zatebradine does not influence the spontaneous activity of O-LM cells in HCN2$^{-/-}$ mice. Effect of zatebradine on the spontaneous spiking activity of O-LM cells from control and HCN2$^{-/-}$ mice. Kynurenic acid (2 mM) was present throughout the experiment. Left panels show representative recordings prior and after application of zatebradine. The right panel illustrates the mean decrease in spiking frequency ($\Delta F=F_{basal}-F_{zatebradine}$) induced by the $I_h$ channel blocker. All data were normalized to the basal frequency ($F_{basal}$) of spontaneous spiking prior to the application of zatebradine ($\Delta F/F_{basal}$). Scale bars correspond to 500 ms and 20 mV.

In the whole-cell current-clamp configuration about ⅓ of O-LM interneurons displayed spontaneous activity (Figure 24) when the experimental conditions were set accordingly (see 2.4.3.1). The HCN channel inhibitor zatebradine (50 µM) reduced the frequency of spontaneous activity significantly ($p<0.01$) in O-LM cells of control mice ($\Delta F/F_{basal}$ 0.32 ± 0.05, n=12), whereas it had no effect in HCN2$^{-/-}$ mice ($\Delta F/F_{basal}$ -0.04 ± 0.12, n=6).

# 4 Discussion

The hippocampal expression of HCN1 channels is confined to the **slm** where the distal dendrites of CA1 pyramidal cells receive glutamatergic inputs from the thalamus and the entorhinal cortex (Lorincz et al., 2002). The leak current of the HCN1 channel constitutively active at resting membrane potential acts as a voltage shunt selectively attenuating distally evoked EPSPs (Magee, 1998). Accordingly, LTP in HCN1 null mutants ($HCN1^{-/-}$) is exclusively enhanced in the synapses of the direct PP located in the **slm**, whereas the SC inputs projecting to the proximal dendrites of CA1 pyramidal cells are not affected (Nolan et al., 2004). Similar to the HCN1 subunit, HCN2 channels exhibit their highest hippocampal expression in the **slm** (3.1). Reflecting this expression pattern, mice lacking the HCN2 channel ($HCN2^{-/-}$) show increased LTP in the PP but not in the SC, suggesting corresponding roles for the HCN1 and HCN2 channel subunits in the modulation of dendritic integration in pyramidal neurons. However, conditional knockout mice lacking the HCN2 gene selectively in pyramidal neurons ($HCN2^{PyrKO}$) exhibit normal LTP in the PP (3.3.3). This proposes that the HCN2-associated function for synaptic plasticity in the PP is largely independent of channels expressed in distal dendrites of postsynaptic CA1 pyramidal neurons.

Alterations of basal transmission properties were ruled out as a possible source for unaltered LTP in the PP of $HCN2^{PyrKo}$ animals (3.3.2). Neither the ectopic expression of Cre nor the tissue specific deletion of the HCN2 gene had any influence on I/O relation or PPF when $HCN2^{PyrKO}$ were compared to wild type controls or the other mutant mouse strains. Additionally, several experiments precluded insufficient recombination efficiency of the Cre/loxP system in

$HCN2^{PyrKO}$ mice. First, genomic PCR amplification of DNA isolated from hippocampal tissue revealed an efficient conversion of the L2 into the L1 knockout allele. Furthermore, the remaining L2 DNA in nonpyramidal cells demonstrated the specificity of the knockout system used. Second, Western blot analyses showed strong depletion of hippocampal HCN2 protein levels (3.2), and third, HCN2 immunoreactivity in the **slm** of histological brain sections from $HCN2^{PyrKO}$ mice was absent (3.1).

Importantly, it was shown earlier that the Nex promoter fragment driving the conditional expression of the Cre-recombinase is inactive in inhibitory interneurons (Goebbels et al., 2006). In addition, residual immunoreactivity in the hippocampus of $HCN2^{PyrKO}$ mice (3.1) matching the location of local inhibitory interneurons was detected (Freund and Buzsaki, 1996; Klausberger, 2009). These findings promoted the idea, that HCN2 channels constrain LTP in the PP by facilitating the inhibitory output from local interneurons targeting the distal dendrites of CA1 pyramidal cells. Due to the deletion of the channel, $HCN2^{-/-}$ mice show a state of disinhibition ultimately responsible for enhanced LTP. Indeed, it has been shown that decreased feed forward inhibition promotes LTP in the SC (Ormond and Woodin, 2009).

Appropriately, simulation of disinhibition by the $GABA_A$ receptor-antagonist picrotoxin (PiTX) did not affect LTP in the PP of the mutants, while in controls PiTX increased LTP to levels observed in $HCN2^{-/-}$ mice (3.5.1). Likewise, PiTX increased basal synaptic transmission in the SC pathway of $HCN2^{-/-}$ mice but had no effect on the PP. In the wild type, basal synaptic transmission of both pathways was PiTX-sensitive (3.5.2). Additionally, the frequency of sIPSCs recorded in CA1 pyramidal neurons of $HCN2^{-/-}$ mice was significantly reduced compared to controls,

providing further evidence for decreased activity of local GABAergic interneurons. This finding is related to the deletion of HCN2, since the selective $I_h$ blocker zatebradine virtually abolished the difference between both genotypes (3.5.3).

Hippocampal inhibitory interneurons represent an inhomogeneous cell population. In the CA1 region, about twelve functionally different interneuronal cell-types are described (Maccaferri and Lacaille, 2003; Klausberger, 2009). It is not known which type or types of interneurons are potentially involved in the HCN2-mediated regulation of LTP in the PP. However, $I_h$ currents were found in lacunosum moleculare interneurons, *stratum radiatum* interneurons, and several oriens/alveus interneurons including oriens-lacunosum moleculare interneurons (Maccaferri and McBain, 1996; Ali and Thomson, 1998; Chapman and Lacaille, 1999; Lupica et al., 2001; Aponte et al., 2006). Oriens-lacunosum moleculare (O-LM) interneurons are especially good candidates for the HCN2-mediated regulation of LTP in the PP since their somas and dendrites are located in the **so** where they are innervated by CA1 pyramidal neurons. However, the axon branches of O-LM cells are restricted to the **slm**, where they selectively inhibit the synapses of the PP (Blasco-Ibanez and Freund, 1995; Katona et al., 1999; Mittmann et al., 2004; Pouille and Scanziani, 2004). Given these unique features, further analysis was focused on the O-LM interneurons potentially regulating synaptic plasticity in the PP.

Several findings in this study suggest that O-LM interneurons indeed contribute to HCN2-mediated suppression of LTP in the PP. In both wild type and $HCN2^{PyrKO}$ animals HCN2 was found to co-localize with somatostatin in the somas of **so** interneurons (3.4). Somatostatin is a neuropeptide serving as marker for O-LM cells (Naus and Bloom, 1988; Baude et al., 1993; Maccaferri et al., 2000; Oliva et

al., 2000; Klausberger et al., 2003). Additionally, HCN2 channels contributed significantly to $I_h$ currents recorded from O-LM cells (3.6.2), as demonstrated by the hyperpolarized membrane potential found in the $HCN2^{-/-}$ mice (3.6.3). In line with this finding, the $I_h$ blocker zatebradine reduced spontaneous spiking and sIPSCs of O-LM cells and pyramidal cells respectively in wild type, but not in $HCN2^{-/-}$ mice (3.6.4). Together, these findings clearly suggest that HCN2 channels strengthen the inhibitory output from O-LM interneurons although the contribution of other HCN2-expressing interneurons cannot be excluded. However, if HCN2 channels were regulating the function of interneurons projecting to proximal or perisomatic regions of CA1 pyramidal cells, alterations of LTP would be expected in the SC of $HCN2^{-/-}$ mice. So far, HCN2 channels exclusively influenced synaptic plasticity in the PP, underscoring their functional impact in interneurons connected to distal dendrites of CA1 pyramidal cells. Alternatively, interneurons in the **slm** could exert feed-forward inhibition (cf. Elfant et al., 2008), but at least a subpopulation of these neurons is not involved, as blocking $I_h$ currents does not influence their intrinsic firing (Chapman and Lacaille, 1999). However, the potential function of $I_h$ in **slm** interneurons remains to be elucidated. Furthermore, non-uniform innervation of hippocampal pyramidal neurons could be considered. It is feasible that CA1 pyramidal cells densely targeted by PP afferents are predominantly inhibited by O-LM cells.

How can the reduction of inhibitory activity in general and reduced GABAergic output from O-LM cells in particular boost synaptic plasticity in the PP? For instance, the propagation of dendritic spikes in distal synapses might be facilitated, an effect possibly strengthened by cooperative activity of more proximal SC synapses (for review see Spruston, 2008). Furthermore, reduced GABAergic input

in the **slm** allows the increased back-propagation of action potentials (Spruston et al., 1995; Markram et al., 1997) to the apical tuft of pyramidal cells, resulting in the potentiation of synapses from the entorhinal cortex that are active during CA1 ripple oscillations *in vivo* and facilitate LTP in the corresponding inputs *in vitro*. An important portion of inhibition directed onto the distal dendrites of CA1 pyramidal cells is provided by O-LM interneurons in a feedback loop (Lacaille et al., 1987; Blasco-Ibanez and Freund, 1995; Maccaferri and McBain, 1995) and perhaps due to spontaneous activity. O-LM cells develop sustained inhibition proportional to the rate of incoming action potentials (Pouille and Scanziani, 2004), thereby saturating inhibitory output to distal dendrites of CA1 pyramidal cells in response to their repetitive activation. Thus, decreased feedback inhibition during repetitive stimulation of PP afferents may account for the increased LTP in $HCN2^{-/-}$ mice. Just as well, changes in the passive cable properties of O-LM cells in knockout animals could disturb the accurate timing of inhibitory feedback-transmission necessary for controlling the frequency and timing of action potential initiation in principal neurons (Norenberg et al., 2010). In addition, others have shown that $I_h$ currents support the spontaneous activity of O-LM cells (Maccaferri and McBain, 1996; Lupica et al., 2001). A recent study demonstrated that lamotrignine (a presumable $I_h$ stimulator) enhanced spontaneous activity in **so** interneurons and simultaneously increased the frequency of sIPSCs in CA1 pyramidal neurons (Peng et al., 2010).

The present study highlights the HCN2 channel as a key player in the regulation of O-LM cell excitability. How do HCN2 channels activate O-LM interneurons and thereby strengthen their output onto pyramidal cells? $I_h$ modulates cellular properties including spontaneous activity, resting membrane potential, input resistance, afterpotential, rebound activity, and dendritic integration (Pape, 1996;

Magee, 2000; for review see Biel et al., 2009). All of these functions may strongly depend on the intracellular localization of the HCN channels. Hyperpolarization of the resting membrane potential as observed in O-LM cells of HCN2-deficient mice is assumed to reduce excitability. Concurrently, the elimination of the depolarizing conductance increases the input resistance of the cell, leading to enhanced excitability (Ludwig et al., 2003). The latter effect predominates for dendritically expressed HCN channels. In contrast, somatically expressed HCN channels are thought to facilitate neuronal excitability (Geiger et al., 1997; Torborg et al., 2006; Norenberg et al., 2010). Our immunohistochemical findings indeed indicate somatic expression of the HCN2 channel (also in contrast to HCN1) in O-LM interneurons agreeing with the view that it supports the activity of these cells (3.4). On the other hand, O-LM cells of $HCN2^{-/-}$ mice had a significantly increased input resistance arguing for increased excitability (3.6.3). Further, the present data demonstrates that the HCN1 channel has a different expression pattern and, likely, function in O-LM cells. Experiments in $HCN1^{-/-}$ mice reveal that synaptic transmission in the PP is still susceptible to PiTX and that the frequency of sIPSCs is not significantly altered in comparison to wild type animals (3.5.2).

Presently, it can only be speculated about the *in vivo* relevance of disinhibition-induced alterations in the synaptic plasticity of HCN2-deficient mice. There is compelling evidence that appropriate storage of spatial information in the hippocampus relies on PP inputs from the entorhinal cortex (Brun et al., 2002; Remondes and Schuman, 2004; Brun et al., 2008) that are thought to fine-tune the environmental representation by hippocampal place cells in the CA1 region. Recent findings in HCN1-deficient mice not only underline the function of the PP in spatial learning but also suggest a functional link to synaptic plasticity in this pathway (Nolan et al., 2004). Despite the fact that mechanisms underlying

regulation of synaptic plasticity in CA1 pyramidal cells by HCN1 (modulates dendritic integration in distal dendrites) and HCN2 (modulates inhibition of distal dendrites) channels apparently differ, one may predict a similar effect on hippocampus-dependent learning. Actually, there is convincing evidence regarding a functional link between activity of GABAergic interneurons, LTP and hippocampus-dependent learning. For example, in a mouse neurofibromatosis model, deficits in spatial learning are caused by increased activity of GABAergic interneurons leading to decreased LTP (Costa et al., 2002; Cui et al., 2008). Also, fmr1 (fragile X mental retardation 1) knockout mice display alterations in subicular synaptic plasticity in response to changes in inhibitory signal transmission (Curia et al., 2009).

An interneuron-specific conditional knockout mouse could provide further insight on the influence of HCN2 for the function of inhibitory interneurons. These mice could be obtained by crossbreeding a mouse expressing Cre in inhibitory interneurons (Monory et al., 2006) with the floxed HCN2 mouse ($HCN2^{L2/L2}$). Additionally, the exact type of interneuron involved in the inhibition of PP inputs might be identified by comparing IPSCs in pyramidal neurons of the different HCN2 genotypes after electric stimulation of individual interneurons in different hippocampal layers.

# 5 Summary

## *5.1 English*

Neuronal hyperpolarization-activated cyclic nucleotide-gated (HCN) channels modulate spontaneous activity, resting membrane potential, input resistance, afterpotential, rebound activity, and dendritic integration. Within the hippocampus, HCN1 and HCN2 are highly expressed in the *stratum lacunosum moleculare*. HCN1 was shown to modulate dendritic integration in distal dendrites of CA1 pyramidal neurons constraining long-term potentiation (LTP) in the direct perforant path (PP). This study analyzes the role of HCN2 for hippocampal LTP. Resembling the phenotype of HCN1-deficient mice, LTP was selectively enhanced in the PP but not the Schaffer collateral pathway of HCN2 deficient mice ($HCN2^{-/-}$). Contrary to the HCN1 channel, ablation of the HCN2 gene in glutamatergic hippocampal neurons did not alter LTP in PP inputs, thereby ruling out a critical role of HCN2 for dendritic integration in CA1 pyramidal neurons. Following findings support the hypothesis that HCN2 channels in oriens-lacunosum moleculare (O-LM) interneurons facilitate the GABAergic output onto distal dendrites of CA1 pyramidal neurons. The $GABA_A$ receptor-antagonist picrotoxin increased LTP in the direct perforant path of wild type, but not $HCN2^{-/-}$ mice, eliminating the genotype difference observed with intact inhibition. Unlike wild type, $HCN2^{-/-}$ mice lacked the picrotoxin-induced increase of basal synaptic transmission in PP inputs. In wild type but not $HCN2^{-/-}$ mice, the selective $I_h$ blocker zatebradine reduces the spontaneous activity of presynaptic O-LM interneurons and the frequency of spontaneous inhibitory postsynaptic currents in CA1 pyramidal neurons.

## *5.2 Deutsch*

Der hyperpolarisationsaktivierte, von zyklischen Nukleotiden gesteuerte Kationenkanal Typ 2 (HCN2) ist stark in den distalen Dendriten der CA1 Pyramidenzellen de Hippocampus exprimiert. Spezifische Deletion von HCN2 in diesen Zellen verstärkt nicht die Langzeitpotenzierung (LTP) des direkten perforanten Eingangs (PP), was eine Funktion von HCN2 für die dendritische Integration in diesen Zellen ausschließt. Ein Inhibitor des $GABA_A$-Rezeptors verstärkt die LTP nur im PP von Kontrollen, aber nicht von HCN2 Knockout-Mäusen ($HCN2^{-/-}$). Im Vergleich zu Kontrollen ist die Frequenz spontaner inhibitorischer postsynaptischer Ströme in CA1 Pyramidenzellen von $HCN2^{-/-}$-Mäusen erniedrigt, einhergehend mit einer Reduktion der Spontanaktivität inhibitorischer Interneurone. Diese Arbeit zeigt, das HCN2 die synaptische Plastizität im PP durch die Unterstützung der Aktivität inhibitorischer Interneurone moduliert.

# 6 Appendix

## 6.1 Abbreviations

| | |
|---|---|
| + | wild type allele |
| aCSF | artificial cerebrospinal fluid |
| α-HCN1 | antibody against HCN1 |
| α-HCN2 | antibody against HCN2 |
| α-SOM | antibody against somatostatin |
| AMPA | α-amino-3-hydroxyl-5-methyl-4-isoxazole-propionate |
| AP-5 | (*2R*)-amino-5-phosphonopentanoate |
| APS | ammonium persulfate |
| BSA | bovine serum albumin |
| c | concentration in moles per volume |
| CA1-CA4 | areas *cornu ammonis* 1-4 |
| CamKII | $Ca^{2+}$/Calmodulin dependent kinase II |
| cAMP | cyclic adenosine monophosphate |
| CNBD | cyclic nucleotide binding domain |
| CNS | central nervous system |
| Cre | Cre (cyclization recombination) recombinase |
| ctx | cortex |
| DAB | 3,3'-diaminobenzidine |
| dd$H_2O$ | double distilled water |
| **DG** | dentate gyrus |
| DHPG | (S)-3,5-dihydroxyphenylglycine |
| DIC | difference interference contrast |
| DNA | deoxyribonucleic acid |
| DNQX | 6,7-Dinitroquinoxaline-2,3-dione |
| dNTP | deoxynucleotide triphosphate |
| DTT | 1,4-dithiothreitol |
| EC | entorhinal cortex |
| ECII | layer II of the entorhinal cortex |
| ECIII | layer III of the entorhinal cortex |
| ECL | Enhanced chemiluminescent |
| EDTA | ethylenediaminetetraacetic acid |
| EGTA | ethylene glycol tetraacetic acid |
| EPSP | excitatory postsynaptic potential |
| ES | embryonic stem cell |
| F | frequency |
| fEPSP | field EPSP |
| GABA | γ-amminobutyric acid |
| $G_q$ | hydrolytic subunit of the heterotrimeric G protein |
| $G_{rel}$ | relative conductance |
| H.M. | patient Henry Molaison |
| $HCN1^{-/-}$ | global HCN1 knockout |
| HCN1-HCN4 | hyperpolarization-activated cyclic nucleotide-gated cation channel subtypes 1-4 |
| $HCN2^{-/-}$ | global HCN2 knockout |
| $HCN2^{PyrCtr}$ | controls for the pyramidal neuron specific conditional HCN2 knockout |
| $HCN2^{PyrKO}$ | pyramidal neuron specific conditional HCN2 knockout |
| HCN-DKO | global knockout of HCN1 and HCN2 |
| HEPES | 4-(2-hydroxyethyl)-1-piperazineethanesulfonic acid |
| hippo | hippocampus |
| HRP | horseradish peroxidase |
| I | current |
| I/O relation | input-output relation |
| $I_h$ | hyperpolarization-activated current |
| KYNA | kynurenic acid |
| L1 | HCN2 null allele |
| L2 | loxP flanked HCN2 allele |
| loxP | locus of X-over P1 |
| LTP | long-term potentiation |
| M | moles per liter |
| MeOH | methanol |
| mGluR | metabotropic glutamate receptor |
| mGluR1 | mGluR subtype 1 |
| MW | molecular weight |
| NEX | neuronal helix-loop-helix protein |

| | |
|---|---|
| Nex-Cre | Mouse expressing Cre recombinase under control of the NEX promoter |
| NGS | normal goat serum |
| NMDA | N-Methyl-D-aspartic acid |
| O-LM | oriens-lacunosum moleculare interneuron |
| PBS | phosphate-buffered saline |
| PCR | polymerase chain-reaction |
| PFA | paraformaldehyde |
| PiTX | picrotoxin |
| PK | proteinase K |
| PP | direct perforant path |
| PPF | paired-pulse facilitation |
| PVDF | polyvinyliden difluoride |
| RMP | resting membrane potential |
| RT | room temperature |
| SC | schaffer-collateral pathway |
| SDS | sodium dodecyl sulfate |
| sIPSC | spontaneous inhibitory post-synaptic potential |
| sk | skeletal muscle |
| **slm** | *stratum lacunosum moleculare* |
| **sm** | *stratum moleculare* |
| **so** | *stratum oriens* |
| SOM | somatostatin |
| **sp** | *stratum pyramidale* |
| **sr** | *stratum radiatum* |
| TBE | Tris-borate-EDTA buffer |
| TBS | Tris-buffered saline |
| TBS-T | Tris-Tween-buffered saline |
| TE | Tris-EDTA buffer |
| TEMED | N,N,N',N'-tetramethyl-ethylenediamine |
| th | thalamus |
| Thr | threshold for action potential initiation |
| TP | *tractus perforans* |
| Tris | 2-amino-2-hydroxymethyl-1,3-propanediol |
| TSA | tyramide signal amplification |
| V | voltage |
| $V_{0.5}$ | voltage of half-maximal channel activation |
| w/v | concentration as weight per volume |
| xg | times g (free-fall acceleration) |

## *6.2 Antibodies*

### 6.2.1 Primary antibodies

| Name | Species | Supplier | Dilution |
|---|---|---|---|
| α-HCN1 | Rabbit | Alomone, Jerusalem | 1:500 |
| α-HCN2 | Rabbit | Alomone, Jerusalem | 1:500 |
| α-Somatostatin | Rat | Milipore, Billerica | 1:100 |

### 6.2.2 Secondary antibodies

| Name | Species | Supplier | Dilution |
|---|---|---|---|
| Peroxidase-conjugated α-Rabbit | Donkey | Jackson Immunoresearch, Newmarket | 1:1000 |
| FITC-conjugated α-Rat | Donkey | Jackson Immunoresearch, Newmarket | 1:100 |

## *6.3 Primers*

| Gene | Primer name | Sequence |
|---|---|---|
| HCN1 | oIMR3410 | 5`-CAC CTG CTA CGC AAT GTT TG -3` |
| | oIMR3411 | 5`-ATT GGG CAC TAC ACG CTA GG -3` |
| | oIMR3412 | 5`-AGA GAA ATC ATT CCC CGT GA -3` |
| HCN2 | HCN2 14F | 5`-GGT CCC AGG CAC TTC CAT CCT TT -3` |
| | HCN2 15bR | 5`-GGA AAA ATG GCT GCT GAG CTG TCT C-3` |
| | HCN2 16F | 5`-CAG CTC CCA TTT GCC CTT GTG C -3` |
| NexCre | NEX1 | 5‘-GTA AAT TAA GGT TAA AGA ACC A-3‘ |
| | RF 113 | 5‘-AGT ATG TGG AGT AGG GTG AC-3‘ |
| | RF 114 | 5‘-CCG CAT AAC CAG TGA AAC AG-3’ |

# 7 References

Ali AB, Thomson AM (1998) Facilitating pyramid to horizontal oriens-alveus interneurone inputs: dual intracellular recordings in slices of rat hippocampus. J Physiol 507 ( Pt 1):185-199.

Aponte Y, Lien CC, Reisinger E, Jonas P (2006) Hyperpolarization-activated cation channels in fast-spiking interneurons of rat hippocampus. J Physiol 574:229-243.

Ascher P, Nowak L (1986) A patch-clamp study of excitatory amino acid activated channels. Adv Exp Med Biol 203:507-511.

Bader CR, Macleish PR, Schwartz EA (1979) A voltage-clamp study of the light response in solitary rods of the tiger salamander. J Physiol 296:1-26.

Bailey CH, Bartsch D, Kandel ER (1996) Toward a molecular definition of long-term memory storage. Proc Natl Acad Sci U S A 93:13445-13452.

Baruscotti M, Bucchi A, Difrancesco D (2005) Physiology and pharmacology of the cardiac pacemaker ("funny") current. Pharmacol Ther 107:59-79.

Baude A, Nusser Z, Roberts JD, Mulvihill E, McIlhinney RA, Somogyi P (1993) The metabotropic glutamate receptor (mGluR1 alpha) is concentrated at perisynaptic membrane of neuronal subpopulations as detected by immunogold reaction. Neuron 11:771-787.

Beaumont V, Zucker RS (2000) Enhancement of synaptic transmission by cyclic AMP modulation of presynaptic Ih channels. Nat Neurosci 3:133-141.

Bender RA, Brewster A, Santoro B, Ludwig A, Hofmann F, Biel M, Baram TZ (2001) Differential and age-dependent expression of hyperpolarization-activated, cyclic nucleotide-gated cation channel isoforms 1-4 suggests evolving roles in the developing rat hippocampus. Neuroscience 106:689-698.

Biel M, Wahl-Schott C, Michalakis S, Zong X (2009) Hyperpolarization-activated cation channels: from genes to function. Physiol Rev 89:847-885.

Blasco-Ibanez JM, Freund TF (1995) Synaptic input of horizontal interneurons in stratum oriens of the hippocampal CA1 subfield: structural basis of feed-back activation. Eur J Neurosci 7:2170-2180.

Bliss TV, Lomo T (1973) Long-lasting potentiation of synaptic transmission in the dentate area of the anaesthetized rabbit following stimulation of the perforant path. J Physiol 232:331-356.

Brown HF, Giles W, Noble SJ (1977) Membrane currents underlying activity in frog sinus venosus. J Physiol 271:783-816.

Brown HF, DiFrancesco D, Noble SJ (1979) How does adrenaline accelerate the heart? Nature 280:235-236.

Brun VH, Otnass MK, Molden S, Steffenach HA, Witter MP, Moser MB, Moser EI (2002) Place cells and place recognition maintained by direct entorhinal-hippocampal circuitry. Science 296:2243-2246.

Brun VH, Leutgeb S, Wu HQ, Schwarcz R, Witter MP, Moser EI, Moser MB (2008) Impaired spatial representation in CA1 after lesion of direct input from entorhinal cortex. Neuron 57:290-302.

Bucchi A, Barbuti A, Baruscotti M, DiFrancesco D (2007) Heart rate reduction via selective 'funny' channel blockers. Curr Opin Pharmacol 7:208-213.

Chapman CA, Lacaille JC (1999) Intrinsic theta-frequency membrane potential oscillations in hippocampal CA1 interneurons of stratum lacunosum-moleculare. J Neurophysiol 81:1296-1307.

Chen J, Mitcheson JS, Lin M, Sanguinetti MC (2000) Functional roles of charged residues in the putative voltage sensor of the HCN2 pacemaker channel. J Biol Chem 275:36465-36471.

Cheung TH, Cardinal RN (2005) Hippocampal lesions facilitate instrumental learning with delayed reinforcement but induce impulsive choice in rats. BMC Neurosci 6:36.

Collingridge GL, Kehl SJ, McLennan H (1983) The antagonism of amino acid-induced excitations of rat hippocampal CA1 neurones in vitro. J Physiol 334:19-31.

Costa RM, Federov NB, Kogan JH, Murphy GG, Stern J, Ohno M, Kucherlapati R, Jacks T, Silva AJ (2002) Mechanism for the learning deficits in a mouse model of neurofibromatosis type 1. Nature 415:526-530.

Cui Y, Costa RM, Murphy GG, Elgersma Y, Zhu Y, Gutmann DH, Parada LF, Mody I, Silva AJ (2008) Neurofibromin regulation of ERK signaling modulates GABA release and learning. Cell 135:549-560.

Curia G, Papouin T, Seguela P, Avoli M (2009) Downregulation of tonic GABAergic inhibition in a mouse model of fragile X syndrome. Cereb Cortex 19:1515-1520.

DiFrancesco D (1982) Block and activation of the pace-maker channel in calf purkinje fibres: effects of potassium, caesium and rubidium. J Physiol 329:485-507.

Dodt HU, Zieglgansberger W (1990) Visualizing unstained neurons in living brain slices by infrared DIC-videomicroscopy. Brain Res 537:333-336.

Douglas RM, Goddard GV (1975) Long-term potentiation of the perforant path-granule cell synapse in the rat hippocampus. Brain Res 86:205-215.

Elfant D, Pal BZ, Emptage N, Capogna M (2008) Specific inhibitory synapses shift the balance from feedforward to feedback inhibition of hippocampal CA1 pyramidal cells. Eur J Neurosci 27:104-113.

Ferraguti F, Cobden P, Pollard M, Cope D, Shigemoto R, Watanabe M, Somogyi P (2004) Immunolocalization of metabotropic glutamate receptor 1alpha (mGluR1alpha) in distinct classes of interneuron in the CA1 region of the rat hippocampus. Hippocampus 14:193-215.

Freund TF, Buzsaki G (1996) Interneurons of the hippocampus. Hippocampus 6:347-470.

Frey U, Krug M, Reymann KG, Matthies H (1988) Anisomycin, an inhibitor of protein synthesis, blocks late phases of LTP phenomena in the hippocampal CA1 region in vitro. Brain Res 452:57-65.

Gauss R, Seifert R, Kaupp UB (1998) Molecular identification of a hyperpolarization-activated channel in sea urchin sperm. Nature 393:583-587.

Geiger JR, Lubke J, Roth A, Frotscher M, Jonas P (1997) Submillisecond AMPA receptor-mediated signaling at a principal neuron-interneuron synapse. Neuron 18:1009-1023.

Giese KP, Fedorov NB, Filipkowski RK, Silva AJ (1998) Autophosphorylation at Thr286 of the alpha calcium-calmodulin kinase II in LTP and learning. Science 279:870-873.

Goebbels S, Bormuth I, Bode U, Hermanson O, Schwab MH, Nave KA (2006) Genetic targeting of principal neurons in neocortex and hippocampus of NEX-Cre mice. Genesis 44:611-621.

Gruart A, Munoz MD, Delgado-Garcia JM (2006) Involvement of the CA3-CA1 synapse in the acquisition of associative learning in behaving mice. J Neurosci 26:1077-1087.

Halliwell JV, Adams PR (1982) Voltage-clamp analysis of muscarinic excitation in hippocampal neurons. Brain Res 250:71-92.

Hebb DO (1949) The organisation of behavior. A neurophsychological theory. New York: Wiley.

Katona I, Acsady L, Freund TF (1999) Postsynaptic targets of somatostatin-immunoreactive interneurons in the rat hippocampus. Neuroscience 88:37-55.

Katz LC (1987) Local circuitry of identified projection neurons in cat visual cortex brain slices. J Neurosci 7:1223-1249.

Klausberger T (2009) GABAergic interneurons targeting dendrites of pyramidal cells in the CA1 area of the hippocampus. Eur J Neurosci 30:947-957.

Klausberger T, Magill PJ, Marton LF, Roberts JD, Cobden PM, Buzsaki G, Somogyi P (2003) Brain-state- and cell-type-specific firing of hippocampal interneurons in vivo. Nature 421:844-848.

Lacaille JC, Mueller AL, Kunkel DD, Schwartzkroin PA (1987) Local circuit interactions between oriens/alveus interneurons and CA1 pyramidal cells in hippocampal slices: electrophysiology and morphology. J Neurosci 7:1979-1993.

Lakso M, Sauer B, Mosinger B, Jr., Lee EJ, Manning RW, Yu SH, Mulder KL, Westphal H (1992) Targeted oncogene activation by site-specific recombination in transgenic mice. Proc Natl Acad Sci U S A 89:6232-6236.

Lawrence JJ, Statland JM, Grinspan ZM, McBain CJ (2006) Cell type-specific dependence of muscarinic signalling in mouse hippocampal stratum oriens interneurones. J Physiol 570:595-610.

Lewis AS, Schwartz E, Chan CS, Noam Y, Shin M, Wadman WJ, Surmeier DJ, Baram TZ, Macdonald RL, Chetkovich DM (2009) Alternatively spliced isoforms of TRIP8b differentially control h channel trafficking and function. J Neurosci 29:6250-6265.

Lorincz A, Notomi T, Tamas G, Shigemoto R, Nusser Z (2002) Polarized and compartment-dependent distribution of HCN1 in pyramidal cell dendrites. Nat Neurosci 5:1185-1193.

Losonczy A, Zhang L, Shigemoto R, Somogyi P, Nusser Z (2002) Cell type dependence and variability in the short-term plasticity of EPSCs in identified mouse hippocampal interneurones. J Physiol 542:193-210.

Ludwig A, Zong X, Hofmann F, Biel M (1999) Structure and function of cardiac pacemaker channels. Cell Physiol Biochem 9:179-186.

Ludwig A, Zong X, Jeglitsch M, Hofmann F, Biel M (1998) A family of hyperpolarization-activated mammalian cation channels. Nature 393:587-591.

Ludwig A, Budde T, Stieber J, Moosmang S, Wahl C, Holthoff K, Langebartels A, Wotjak C, Munsch T, Zong X, Feil S, Feil R, Lancel M, Chien KR, Konnerth A, Pape HC, Biel M, Hofmann F (2003) Absence epilepsy and sinus dysrhythmia in mice lacking the pacemaker channel HCN2. Embo J 22:216-224.

Lupica CR, Bell JA, Hoffman AF, Watson PL (2001) Contribution of the hyperpolarization-activated current (I(h)) to membrane potential and GABA release in hippocampal interneurons. J Neurophysiol 86:261-268.

Lynch G, Larson J, Kelso S, Barrionuevo G, Schottler F (1983) Intracellular injections of EGTA block induction of hippocampal long-term potentiation. Nature 305:719-721.

Maccaferri G (2005) Stratum oriens horizontal interneurone diversity and hippocampal network dynamics. J Physiol 562:73-80.

Maccaferri G, McBain CJ (1995) Passive propagation of LTD to stratum oriens-alveus inhibitory neurons modulates the temporoammonic input to the hippocampal CA1 region. Neuron 15:137-145.

Maccaferri G, McBain CJ (1996) The hyperpolarization-activated current (Ih) and its contribution to pacemaker activity in rat CA1 hippocampal stratum oriens-alveus interneurones. J Physiol 497 ( Pt 1):119-130.

Maccaferri G, Lacaille JC (2003) Interneuron Diversity series: Hippocampal interneuron classifications--making things as simple as possible, not simpler. Trends Neurosci 26:564-571.

Maccaferri G, Roberts JD, Szucs P, Cottingham CA, Somogyi P (2000) Cell surface domain specific postsynaptic currents evoked by identified GABAergic neurones in rat hippocampus in vitro. J Physiol 524 Pt 1:91-116.

Magee JC (1998) Dendritic hyperpolarization-activated currents modify the integrative properties of hippocampal CA1 pyramidal neurons. J Neurosci 18:7613-7624.

Magee JC (1999) Dendritic Ih normalizes temporal summation in hippocampal CA1 neurons. Nat Neurosci 2:508-514.

Magee JC (2000) Dendritic integration of excitatory synaptic input. Nat Rev Neurosci 1:181-190.

Malenka RC, Bear MF (2004) LTP and LTD: an embarrassment of riches. Neuron 44:5-21.

Markram H, Lubke J, Frotscher M, Sakmann B (1997) Regulation of synaptic efficacy by coincidence of postsynaptic APs and EPSPs. Science 275:213-215.

McCormick DA, Pape HC (1990) Properties of a hyperpolarization-activated cation current and its role in rhythmic oscillation in thalamic relay neurones. J Physiol 431:291-318.

Miles R, Toth K, Gulyas AI, Hajos N, Freund TF (1996) Differences between somatic and dendritic inhibition in the hippocampus. Neuron 16:815-823.

Miller G (2009) The brain collector. Science 324:1634-1636.

Milner B (1972) Disorders of learning and memory after temporal lobe lesions in man. Clin Neurosurg 19:421-446.

Minneci F, Janahmadi M, Migliore M, Dragicevic N, Avossa D, Cherubini E (2007) Signaling properties of stratum oriens interneurons in the hippocampus of transgenic mice expressing EGFP in a subset of somatostatin-containing cells. Hippocampus 17:538-553.

Mittmann W, Chadderton P, Hausser M (2004) Neuronal microcircuits: frequency-dependent flow of inhibition. Curr Biol 14:R837-839.

Monory K et al. (2006) The endocannabinoid system controls key epileptogenic circuits in the hippocampus. Neuron 51:455-466.

Much B, Wahl-Schott C, Zong X, Schneider A, Baumann L, Moosmang S, Ludwig A, Biel M (2003) Role of subunit heteromerization and N-linked glycosylation in the formation of functional hyperpolarization-activated cyclic nucleotide-gated channels. J Biol Chem 278:43781-43786.

Nagy A (2000) Cre recombinase: the universal reagent for genome tailoring. Genesis 26:99-109.

Naus CC, Bloom FE (1988) Immunohistochemical analysis of the development of somatostatin in the reeler neocortex. Brain Res 471:61-68.

Nolan MF, Malleret G, Lee KH, Gibbs E, Dudman JT, Santoro B, Yin D, Thompson RF, Siegelbaum SA, Kandel ER, Morozov A (2003) The hyperpolarization-activated HCN1 channel is important for motor learning and neuronal integration by cerebellar Purkinje cells. Cell 115:551-564.

Nolan MF, Malleret G, Dudman JT, Buhl DL, Santoro B, Gibbs E, Vronskaya S, Buzsaki G, Siegelbaum SA, Kandel ER, Morozov A (2004) A behavioral role for dendritic integration: HCN1 channels constrain spatial memory and plasticity at inputs to distal dendrites of CA1 pyramidal neurons. Cell 119:719-732.

Noma A, Irisawa H (1976) Membrane currents in the rabbit sinoatrial node cell as studied by the double microelectrode method. Pflugers Arch 364:45-52.

Norenberg A, Hu H, Vida I, Bartos M, Jonas P (2010) Distinct nonuniform cable properties optimize rapid and efficient activation of fast-spiking GABAergic interneurons. Proc Natl Acad Sci U S A 107:894-899.

Notomi T, Shigemoto R (2004) Immunohistochemical localization of Ih channel subunits, HCN1-4, in the rat brain. J Comp Neurol 471:241-276.

O'Keefe J, Dostrovsky J (1971) The hippocampus as a spatial map. Preliminary evidence from unit activity in the freely-moving rat. Brain Res 34:171-175.
O'Keefe J, Conway DH (1978) Hippocampal place units in the freely moving rat: why they fire where they fire. Exp Brain Res 31:573-590.
Oliva AA, Jr., Jiang M, Lam T, Smith KL, Swann JW (2000) Novel hippocampal interneuronal subtypes identified using transgenic mice that express green fluorescent protein in GABAergic interneurons. J Neurosci 20:3354-3368.
Orban PC, Chui D, Marth JD (1992) Tissue- and site-specific DNA recombination in transgenic mice. Proc Natl Acad Sci U S A 89:6861-6865.
Ormond J, Woodin MA (2009) Disinhibition mediates a form of hippocampal long-term potentiation in area CA1. PLoS One 4:e7224.
Pape HC (1996) Queer current and pacemaker: the hyperpolarization-activated cation current in neurons. Annu Rev Physiol 58:299-327.
Peng BW, Justice JA, Zhang K, He XH, Sanchez RM (2010) Increased basal synaptic inhibition of hippocampal area CA1 pyramidal neurons by an antiepileptic drug that enhances I(H). Neuropsychopharmacology 35:464-472.
Pouille F, Scanziani M (2004) Routing of spike series by dynamic circuits in the hippocampus. Nature 429:717-723.
Ramón Cajal S (1895) Algunas conjeturas sobre el mecanismo anatómico de la ideación, asociación y atención. Rev Med Cirug Práct (Madrid) 19:497–508-497–508.
Remondes M, Schuman EM (2004) Role for a cortical input to hippocampal area CA1 in the consolidation of a long-term memory. Nature 431:699-703.
Santoro B, Grant SG, Bartsch D, Kandel ER (1997) Interactive cloning with the SH3 domain of N-src identifies a new brain specific ion channel protein, with homology to eag and cyclic nucleotide-gated channels. Proc Natl Acad Sci U S A 94:14815-14820.
Santoro B, Piskorowski RA, Pian P, Hu L, Liu H, Siegelbaum SA (2009) TRIP8b splice variants form a family of auxiliary subunits that regulate gating and trafficking of HCN channels in the brain. Neuron 62:802-813.
Schwab MH, Bartholomae A, Heimrich B, Feldmeyer D, Druffel-Augustin S, Goebbels S, Naya FJ, Zhao S, Frotscher M, Tsai MJ, Nave KA (2000) Neuronal basic helix-loop-helix proteins (NEX and BETA2/Neuro D) regulate terminal granule cell differentiation in the hippocampus. J Neurosci 20:3714-3724.
Somogyi P, Klausberger T (2005) Defined types of cortical interneurone structure space and spike timing in the hippocampus. J Physiol 562:9-26.
Spruston N (2008) Pyramidal neurons: dendritic structure and synaptic integration. Nat Rev Neurosci 9:206-221.
Spruston N, Schiller Y, Stuart G, Sakmann B (1995) Activity-dependent action potential invasion and calcium influx into hippocampal CA1 dendrites. Science 268:297-300.
Squire LR, Zola-Morgan S (1988) Memory: brain systems and behavior. Trends Neurosci 11:170-175.
Taketo M, Matsuda H (2010) Modulation of intracellular calcium mobilization and GABAergic currents through subtype-specific metabotropic glutamate receptors in neonatal rat hippocampus. Brain Res Bull 81:73-80.
Torborg CL, Berg AP, Jeffries BW, Bayliss DA, McBain CJ (2006) TASK-like conductances are present within hippocampal CA1 stratum oriens interneuron subpopulations. J Neurosci 26:7362-7367.
Ulens C, Tytgat J (2001) Functional heteromerization of HCN1 and HCN2 pacemaker channels. J Biol Chem 276:6069-6072.

Vaca L, Stieber J, Zong X, Ludwig A, Hofmann F, Biel M (2000) Mutations in the S4 domain of a pacemaker channel alter its voltage dependence. FEBS Lett 479:35-40.

Viscomi C, Altomare C, Bucchi A, Camatini E, Baruscotti M, Moroni A, DiFrancesco D (2001) C terminus-mediated control of voltage and cAMP gating of hyperpolarization-activated cyclic nucleotide-gated channels. J Biol Chem 276:29930-29934.

Wahl-Schott C, Biel M (2009) HCN channels: structure, cellular regulation and physiological function. Cell Mol Life Sci 66:470-494.

Wainger BJ, DeGennaro M, Santoro B, Siegelbaum SA, Tibbs GR (2001) Molecular mechanism of cAMP modulation of HCN pacemaker channels. Nature 411:805-810.

Whitlock JR, Heynen AJ, Shuler MG, Bear MF (2006) Learning induces long-term potentiation in the hippocampus. Science 313:1093-1097.

Whittington MA, Traub RD (2003) Interneuron diversity series: inhibitory interneurons and network oscillations in vitro. Trends Neurosci 26:676-682.

Yanagihara K, Irisawa H (1980) Inward current activated during hyperpolarization in the rabbit sinoatrial node cell. Pflugers Arch 385:11-19.

Yu FH, Yarov-Yarovoy V, Gutman GA, Catterall WA (2005) Overview of molecular relationships in the voltage-gated ion channel superfamily. Pharmacol Rev 57:387-395.

Zola-Morgan S, Squire LR (1993) Neuroanatomy of memory. Annu Rev Neurosci 16:547-563.

Zolles G, Wenzel D, Bildl W, Schulte U, Hofmann A, Muller CS, Thumfart JO, Vlachos A, Deller T, Pfeifer A, Fleischmann BK, Roeper J, Fakler B, Klocker N (2009) Association with the auxiliary subunit PEX5R/Trip8b controls responsiveness of HCN channels to cAMP and adrenergic stimulation. Neuron 62:814-825.

# 8 Acknowledgements

I am deeply grateful to Prof Dr. Thomas Kleppisch (*Institute of Pharmacology and Toxicology, TU München*) for the opportunity to perform my thesis in his laboratory and for his supervision of my work.

I am also grateful to Prof. Dr. Harald Luksch (*Lehrstuhl für Zoologie, TU München*) for representing this dissertation to the faculty committee and his interest in my work.
Additionally I want to thank the other members of the committee: Prof. Dr. Michael Schemann (Lehrstuhl für Humanbiologie, TU München) and Prof. Dr. Helmuth Adelsberger (Institut für Neurowissenschaft, TU München).

Special thanks go to Prof. Dr. Franz Hofmann (*Institute of Pharmacology and Toxicology, Forschergruppe 923 Carvas, TU München*) for the opportunity to use the infrastructure of the Institute and for his helpful ideas.

Thanks also go to Prof. Dr. Dr. Engelhardt (*Institute of Pharmacology and Toxicology, TU München*) for his support of my work.

I am much obliged to thank Prof. Dr. Martin Biel (*Department of Pharmacy – Center for Drug Research, LMU München*) for providing the $HCN2^{L2/L2}$ mice and allowing me to perform experiments in his institute. Additionally, I want to thank all the people from his Lab for the nice and interesting times I spent with them. I would like to thank Dr. Martha Schöll-Weidinger and Verena Hammelmann who

helped me with Immunohistochemistry and Western-blotting, respectively. I am especially very grateful to Dr. Stylianos Michalakis for all his help.

I thank Prof. Dr. Andreas Ludwig (*Institut für Experimentelle und Klinische Pharmakologie und Toxikologie, Friedrich-Alexander-Universität Erlangen-Nürnberg*) for providing the $HCN2^{-/-}$ mice.

Many thanks go to my colleagues from the Institute of Pharmacology and Toxicology. I am grateful to Urszula Kremser, Sabine Brummer, Teodora Kennel, and Mehmet Durmaz for their technical support and Gabriele Günther-Blab for her generous treatment of the animals.

I thank Carl Christel for helping me with my career.

Particularly, I am deeply grateful to Veronika Leiss and Robert Lukowski who became very good friends.

Above all, a huge thank-you goes to Eva. You are of the greatest importance to me.

Vielen Dank an meine Familie für all die Unterstützung, die ich erhalten habe. Der allergrößte Dank aber gebührt meinen Eltern. Ohne Euch, liebe Eltern, wäre ich nie in der Lage gewesen, diese Dissertation anzufertigen.

Thank you all!

# 9 Curriculum vitae

## *Education*

| | |
|---|---|
| From 2010 | Postdoctoral fellow with Prof. Dr Johannes Hell in the Department of Pharmacology, University of California at Davis, Director: Prof. Dr. Donald Bers. |
| 2007–2010 | PhD project as research assistant at the Institute of Pharmacology and Toxicology, Technische Universität München (TUM), Director: Prof. Dr. Franz Hofmann, since October 2008 Prof. Dr. Dr. Stefan Engelhardt. Dissertation: "HCN2 channels in local hippocampal inhibitory interneurons constrain temporoammonic LTP". Advisor: Prof. Dr. Thomas Kleppisch. Supervisor: Prof. Dr. Harald Luksch, Chair of Zoology, TUM. |
| 2004–2006 | Master of Science in Biochemistry, TUM. Final grade: "passed with merit (1.8)". Master thesis at the Institute of Pharmacology and Toxicology: „Die Rolle des HCN2 Kanals für die synaptische Plastizität im Hippocampus". Advisor: Prof. Dr. Thomas Kleppisch. |
| 2001–2004 | Bachelor of Science in Biochemistry, TUM. Bachelor thesis at the Institute for Clinical Chemistry and Pathobiochemistry, University Hospital Rechts der Isar: "Etablierung eines Surface-Plasmon-Resonance-Biosensors zur Diagnostik des Anti-Phopholipid-Syndroms". Advisor: Prof. Dr. Peter B. Luppa; Director: Prof. Dr. D. Neumeier. |
| 1999–2001 | Intermediate diploma in Chemistry. University of Zurich. |
| 1991–1999 | General qualification for university entrance. (Eidgenössische Matura, Typus B). Liechtensteinisches Gymnasium, Vaduz. |

# Publications and Presentations

## *Articles*

L. Matt, S. Michalakis, F. Hofmann, V. Hammelmann, A. Ludwig, M. Biel, T. Kleppisch. (2010). "HCN2 channels in local inhibitory interneurons constrain LTP in the hippocampal direct perforant path". Cell Mol Life Sci. *In press.*

S. Michalakis, T. Kleppisch, C. Wotjak, G. Rammes, L. Matt, E. Becirovic, M. Biel (2010). "Altered synaptic plasticity and behavioral abnormalities in CNGA3-deficient mice". Revised m*anuscript under review.*

## *Abstracts*

L. Matt, S. Michalakis, M. Biel, A. Ludwig, F. Hofmann, T. Kleppisch (2009). "Inhibition of LTP in the temporoammonic input to CA1 pyramidal cells is modulated by HCN2 in stratum oriens interneurons". *Naunyn-Schmiedebergs Archives of Pharmacology* 379: 45.

L. Matt, S. Michalakis, M. Weidinger, M. Biel, A. Ludwig, F. Hofmann, T. Kleppisch (2008). "Temporo-ammonic LTP is modulated by HCN2 channels in stratum oriens interneurons". *Naunyn-Schmiedebergs Archives of Pharmacology*, 377: 47.

L. Matt, S. Michalakis, M. Weidinger, M. Biel, A. Ludwig, F. Hofmann, T. Kleppisch (2007). "HCN2 channels in hippocampal interneurons modulate long-term potentiation in the temporo-ammonic pathway". *Naunyn-Schmiedebergs Archives of Pharmacology,* 375: 57.

## *Presentations*

| | |
|---|---|
| March 10–12, 2009 | Talk. *50th Annual Meeting of the German Pharmacological Society* (Mainz, Germany). |
| March 11–13, 2008 | Talk. *49th Annual Meeting of the German Pharmacological Society* (Mainz, Germany). |
| February 10–12, 2008 | Poster. *International Symposium on Learning, Memory and Cognitive Function* (Valencia, Spain). |
| March 13–15, 2007 | Poster. *48th Annual Meeting of the German Pharmacological Society* (Mainz, Germany). |